DESIGN AND EVALUATION OF AN ADVANCED ADIABATIC COMPRESSED AIR ENERGY STORAGE SYSTEM AT THE MICHIGAN-UTAH MINE

by

Michael Beeman

A thesis submitted to the faculty of
The University of Utah
in partial fulfillment of the requirements for the degree of

Master of Science

Department of Mechanical Engineering

The University of Utah

August 2010

The University of Utah Graduate School

STATEMENT OF THESIS APPROVAL

The thesis of **Michael G Beeman**

has been approved by the following supervisory committee members:

Kent Udell	, Chair	**4/19/2010**
Kuan Chen	, Member	**4/22/2010**
Tim Ameel	, Member	**4/22/2010**

and by [redacted], Chair of the Department of **Mechanical** [redacted]

and by Charles A. Wight, Dean of The Graduate School.

ABSTRACT

Compressed air energy storage (CAES) is considered a viable option for matching intermittent sustainable energy and the production of peak electrical demand. Economic advantages of CAES may be realized by storing inexpensive off-peak power at night and on weekends for use during peak hours when electricity prices are high (arbitrage). Traditional CAES facilities use a natural gas burner to heat the air entering the expander. This study examines the feasibility of replacing the natural gas burner with heat exchangers that collect waste heat from the compression cycle and designing an advanced adiabatic compressed air energy storage process that eliminates the need for combustion.

This feasibility study will include the development of a software package called CAES Simulator using the commercial program Matlab©, to model thermodynamic properties of a CAES system. The computational model uses a time series iterative forward differencing method to simulate the operation of a CAES plant. Users enter boundary conditions pertaining to ambient air properties and equipment limitations and CAES Simulator calculates thermodynamic properties of the system such as overall efficiency and thermal loads. CAES Simulator is equipped to consider the psychometric properties of air and the effects of humidity changes caused by condensation during cooling. The computational model was validated experimentally by comparing trended

data of the compression cycle of a 280 HP Gardener-Denver tandem horizontal two stage compressor to computational results.

CAES Simulator was used to identify the effects of changing ambient air properties on the overall efficiency of an AA-CAES system at the Michigan-Utah Mine in Cottonwood Canyon, Utah. Summit County's geological conditions are rich with hard rock, salt formations and aquifers making the area's 1200 miles of abandoned mine a prime candidate for this application. It was found that rises in ambient humidity and temperature increased the operating temperatures and heat recovery requirements of an AA-CAES plant. Utah's cold dry climate allows machinery to operate at lower temperature making the Michigan-Utah Mine an ideal location for an AA-CAES. This study demonstrated that an AA-CAES plant's efficiency is dependent on equipment constants but an efficiency of 75% is obtainable given the right operating conditions.

TABLE OF CONTENTS

LIST OF FIGURES

LIST OF TABLES

NOMENCLATURE

c_p	Specific heat at Constant Pressure
c_v	Specific heat at Constant Volume
g	Gravity
h	Enthalpy
h_{fg}	Latent Heat of Vaporization
k	Isentropic Coefficient
k_c	Coefficient of Thermal Conductivity
m	Mass
r	Pressure Ratio
s	Entropy
t	Time
v	Velocity
u	Internal Energy
z	Height
A	Area
Bi	Biot Number
E_{CV}	Energy within a Control Volume
L_c	Characteristic Length

P_a	Partial Pressure of Dry Air
P_g	Saturation Pressure at Defined Temperature
P_v	Partial pressure of Water Vapor
P	Pressure
Q	Heat Energy
R	Gas Constant
T	Temperature
V	Volume
W	Work
X	Exergy
β	Shape Factor
γ	Polytropic Coefficient
ε	Expansion Coefficient
η	Efficiency
ρ	Density
ϕ	Relative Humidity
ω	Absolute Humidity

ACKNOWLEDGEMENTS

I would like to thank my advisor, Dr. Kent Udell, for providing me with the opportunity to work on this research project. His expertise, guidance, and patience were instrumental in the accomplishments of this work and in the furthering of my education. I would also like to thank my committee members, Dr. Tim Ameel and Dr. Kuan Chen, for their willingness to be involved in this project and answer any questions I might have had. I would also like to thank ETC Group for lending me the equipment I needed to complete the project and allowing me to take the time I needed to finish this work. Finally, a great thanks to my parents, Caren and Dick, for their continued support and encouragement during this period. I could not have achieved this much without them.

CHAPTER 1

INTRODUCTION

1.1 Background

Compressed air energy storage is a developing technology that has the potential to meet the needs of intermittent sustainable energy sources and high peak load electrical power demands. The development of compressed air energy storage has been a slow process with few developments over the past few decades. Currently there are only two plants in operation which use fossil fuel combustion to supplement the energy lost during the cooling phase of the compression cycle. Despite many efforts from manufactures such as General Electric there are currently no adiabatic compressed air systems operating at a municipal scale.

CAES plants currently bring compressed air to the surface, heat it using gas-fired burners, and exhaust it through a gas turbine. Unlike traditional compressed air energy storage systems, advanced adiabatic compressed air energy storage (AA-CAES) cycles eliminate the need for the combustion of natural gas. Advanced adiabatic compressed air energy systems (AA-CAES) eliminate the need for a gas-fired heater by storing the heat energy produced during the compression process. An AA-CAES system is a Brayton

cycle that uses municipal power and thermal energy storage in place of a gas turbine. Refer to Figure 1.1 for a schematic of an AA-CAES Cycle.

Thermal energy produced during compression is removed from the air with the compression cycles 1st and 2nd stage heat exchangers and stored in a thermal energy storage (TES) device. Compression occurs at night when electrical demand and prices are low. The thermal energy is later transferred from the TES to the air using the turbine cycles 1st and 2nd stage heat exchangers. Once heated the air is released through the high pressure and low pressure turbines that drives a generator during peak demand times when electrical prices are high. AA-CAES systems produce no CO_2 emissions and are 70-75% efficient.[1] Currently there are no AA-CAES plants operating above a 100 MW capacity which makes this project unique.

1.2 Literature Review

The concept of compressed air energy storage with gas fired air heating is well proven and has been in use for over 30 years. In 1978 the first CAES facility was built in Huntorf, Germany and has a capacity of 290 MW. The EN Krauftwerke owned German plant stores compressed air in two salt caverns with volumes of 140,000 m^3 and 170,000 m^3. Compression requires 12 hrs to fill the caverns and consume 720 MW-hr of municipal power. The plant injects the compressed air into a natural gas burner before entering the expansion cycle and can generate power for up to 3 hrs. Its two main purposes are to supply supplement power for peak demand loads and produce emergency power. [1]

This technology was later introduced to the US in 1991 with a 110 MW plant in McIntosh, Alabama. Compressed air is stored in a 19,000,000 m^3 salt cavern and can

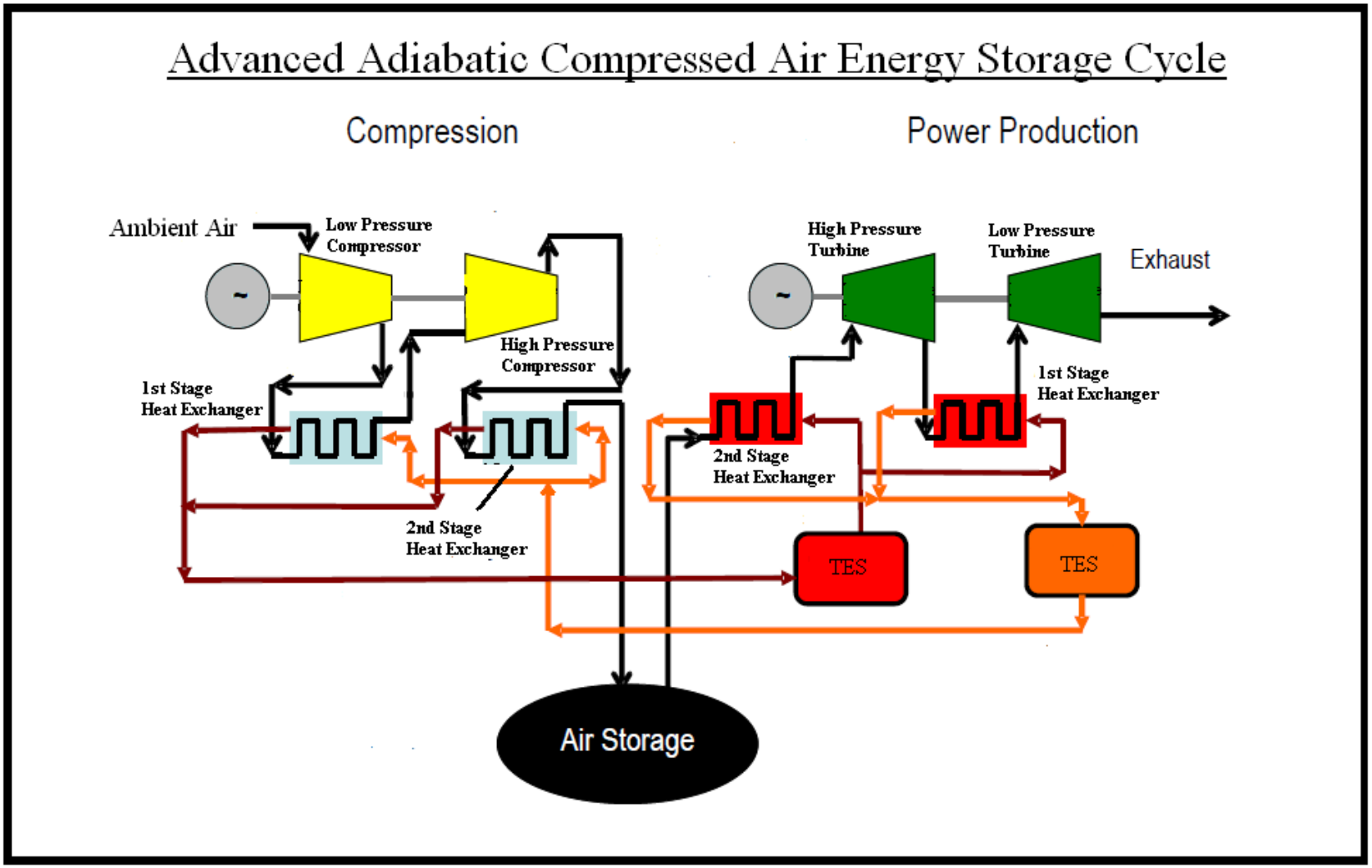

Figure 1-1 Advanced adiabatic compressed air energy storage cycle schematic.

generate power for 26 hrs. The Alabama Electric Cooperative (AEC) improved on the CAES design by recovering waste heat, with the addition of a regenerator, to the expansion cycle reducing fuel consumption by ~25% compared to the Huntorf Plant. Construction of the site cost $65M or approximately $591/kW. [2]

Norton Energy Storage (NES) is in the process of opening a 2700 MW plant in Norton, Ohio but it has been put on hold do to financial problems. The design of the proposed site in Norton, Ohio would use hard rock mines for storage and is comparable to conditions in Cottonwood Canyon, Utah. Steve Bauer, a geologist at Sandia National Laboratories, has conducted a six-month feasibility study to determine if the hard rock mines at the Norton Ohio site can be used for compressed air storage. After the completion of this study he submitted six reports to NES which validated the use of the mines for cyclic pressure vessels.[3] An added benefit to using a hard rock mine shaft is the modularity of expansion by adding additional turbines and sealing additional shafts. NES will bring their plant online in 300 MW increments as units become available.[4]

According to a study conducted by CERI, the capital costs associated with CAES are comparable to natural gas turbines which typically range between $400 and $500/kW. Accounting for the additional equipment and reservoir costs, capital investments will range between $600 and $700/kW.[5] Off-peak power is currently priced at $0.04/kWh and peak prices at $0.07/kWh in Utah. After accounting for plant efficiency, this means power can be sold for $0.03/kWh or a 131% markup. Profits will continue to increase as energy costs rise. AA-CAES technology has been shown to be cost effective but a system that avoids the need for a gas burner will require further research and development before it can be implemented.

1.3 Motivation and Objective

Adiabatic compressed air energy storage is the next generation of CAES systems. Since the conception of CAES, researchers have sought a design that will eliminate the need for a secondary heat source while maintaining adequate plant efficiency. Advancements in thermal energy storage systems have increased the feasibility of using heat exchangers and regenerators in place of fossil fuel combustion for heat before air expansion. The ever increasing demand of clean carbon free reliable energy has created a need to study advanced adiabatic compressed air (AA-CAES) systems.

General Electric and Rheinisch-Westfälisches Elektrizitätswerk AG have signed a Memorandum of Understanding to develop advanced adiabatic compressed air energy storage equipment for commercialization. They began a feasibility study in March of 2008 to devise ways of overcoming technical challenges. A major obstacle is designing compressors capable of handling temperatures in excess of 600 ˚C that remain cost effective. GE and RWE must also design a thermal energy storage system using ceramic brick capable of storing the heat loads from compression and that are able to reduce losses over daily cycles. [6]

The feasibility of AA-CAES plants is dependent on raising the overall efficiency of the plant so it is cost effective to store power. Traditional natural gas fired CAES facilities are 40-60% efficient taking into account the natural gas required to drive the turbines and changing ambient conditions. [7] The proposed efficiency of an AA-CAES plant would be 60-75% accounting for the efficiency of equipment. Raised overall efficiency and the elimination of the need for combustion make an AA-CAES an attractive solution to energy storage.

The Cottonwood Canyon design is based on a 100 MW capacity but will allow room for expansion. With an excess of 1200 miles of abandoned mine shafts, Cottonwood Canyon has enormous storage capacity. Depending on the conditions of the mines for air and thermal energy storage it is feasible that this plant could meet or exceed the 2700 MW storage capacity of the expanded NES site. This means that this project has the potential to produce the largest emissions free compressed air energy storage facility in the world.

CHAPTER 2

METHODOLOGY

2.1 Overview

A critical component of this feasibility study is to maximize plant efficiency by selecting equipment that is optimized for specific environmental conditions. A plant's capacity is limited by the available compressed air storage volume, thermal energy storage capacity and equipment limitations. Since the ambient air is the working fluid, it's thermodynamic properties , such as pressure, temperature and humidity, will affect the performance of the compressed air energy storage facility. These factors must be considered to accurately assess a proposed site's potential or optimize design parameters. The following section introduces the computational simulation software package CAES Simulator that was developed to optimize an AA-CAES at a specific site and outlines the method used to perform this analysis.

2.2 CAES Simulator Theoretical Model

2.2.1 CAES Simulator Computational Model Overview

CAES Simulator uses a time step numerical integration method to find temporal conditions of the compressed air energy system. A mathematical model of the system is divided into the compression, expansion and heat exchanger stages. The model calculates pressure, temperature, and mass flow rates at each stage and time of the cycle. All thermodynamic calculations are performed within CAES Simulator. All calculations are governed by the general conservation equation for transient flow [8],

$$\dot{Q}+\dot{W}_{net}-\sum_{in}\dot{m}_i\left(h+\frac{v^2}{2}+gz\right)_i-\sum_{out}\dot{m}_e\left(h+\frac{v^2}{2}+gz\right)_e=\frac{dE_{CV}}{dt}. \qquad (2.1)$$

The compressor and expander are modeled assuming polytropic expansion and compression. The computational model also assumes constant specific heats unless condensation occurs and that the boundary conditions set by the user do not change over time. The cycle is adiabatic so there is no heat generation at any phase of the cycle. The effects of gravity and momentum are negligible compared to the other terms in the equation and are excluded from calculations. Humid air, the working medium, is modeled using the ideal gas equation of state,

$$PV = mRT \qquad (2\text{-}2)$$

and the relation,

$$Pv^n = const \qquad (2\text{-}3)$$

for ideal gases operating under the assumption of constant specific heats.[1] Section 2.2.2 describes the mass balance equations used to identify the ideal gas constant of the dry air and water vapor mixture. The processes are modeled as polytropic under the assumption that minor irreversibilities will occur. Using these relations CAES Simulator is able to obtain the thermodynamic properties of humid air as it is compressed and expanded through the plant.

2.2.2 Physical Properties of Humid Air

CAES plants operate by drawing ambient air from the atmosphere, which can vary in temperature, pressure and humidity. Water condensation during cooling and expansion can have devastating effects on equipment. For this reason, the CAES Simulator is equipped to calculate psychometric properties of humid air as it passes through different stages of the cycle. This information is used to determine if the humidity ratio has been altered due to condensation. A change in humidity affects thermodynamic properties of air, such as heat capacity, which affect the performance of the compressor and expander. Condensation also produces latent heating which affects heat exchanger calculations.

CAES Simulator begins by finding the specific heat of the humid air using the user defined ambient conditions. Specific heats for humid air are found by inputting the relation for specific humidity (ω),

$$\omega = \frac{m_v}{m_a} \qquad (2\text{-}4)$$

into the specific heat equation for humid air,

$$c = \frac{m_a c_{dryair} + m_v c_{watervapor}}{m_{humidair}} \qquad (2\text{-}5)$$

to obtain,

$$c_p = \frac{c_{p-dryair}}{(1+\omega)} + \frac{\omega c_{p-watervapor}}{(1+\omega)} \qquad (2\text{-}6a)$$

$$c_v = \frac{c_{v-dryair}}{(1+\omega)} + \frac{\omega c_{v-watervapor}}{(1+\omega)} \; . \qquad (2\text{-}6b)$$

The specific heats are then used to find the gas constant (R) for the humid air as [9],

$$R = c_p - c_v \; . \qquad (2\text{-}7)$$

2.2.3 Heat Transfer and Condensation During the Compression Cycle

CAES Simulator performs a condensation check after the air is cooled in the 1st and 2nd stage heat exchangers, which are positioned after each compression and expansion phase of the cycle. Refer to Figure 1-1. Cooling during the heat exchange process is assumed to occur at constant pressure and the air is cooled to a constant temperature in the 1st and 2nd stage heat exchanger. The exit pressure conditions at the 2nd stage compressor differ from the 1st stage compressor. As air exits into the high pressure turbine the pressure in the air storage is reduced. Exit pressures are not held constant due to the changing pressure within the compressed air storage.

The occurrence of condensation must be continually checked as time passes and the air storage pressure increases. This is accomplished by calculating the partial vapor pressure at the exit pressure of the second stage compressor and passing the vapor pressure to a sub function called Saturation_Data_T which is found in the code in Appendix A. Saturation_Data_T scans a library of saturation water tables included in the software package to find the tabulated dew point temperature, at points above and below the given vapor pressure within the table. Saturation_Data_T performs a linear interpolation between the upper and lower vapor pressures tabulated in the table and extrapolates the dew point temperature and latent heat of vaporization.

If it is determined that the vapor condenses, CAES Simulator uses sub function Saturation_Data_P to find the new saturation pressure corresponding to the exit temperature, using the technique described for Saturation_Data_T. The saturation pressure is used to determine a new humidity ratio using the relation,

$$\omega = \frac{0.622 P_v}{P - P_v} . \qquad (2\text{-}8)$$

where the vapor pressure P_v is replaced with the saturation pressure P_g at the exit temperature.[1] The thermodynamic properties of the de-humidified air are then recalculated.

Condensation during the first stage heat exchanger can be confirmed by calculating the relative humidity (ϕ),

$$\phi = \frac{\omega P}{(0.622 + \omega) P_g} \qquad (2\text{-}9)$$

where P is the total pressure and P_g is the saturation pressure at the heat exchanger after the low pressure compressor and high pressure expander exit temperature. Once it has been confirmed that condensation occurs, both heat exchanger stages proceed in a similar manner to find the heat energy transferred. The mass flow rate of the condensed vapor is found by comparing the exit air humidity ratio with the entrance air humidity ratio,

$$\dot{m}_{condensedwater} = \left(\frac{\omega_{entrance}}{\omega_{entrance} - 1} - \frac{\omega_{exit}}{\omega_{exit} - 1} \right) \dot{m}_{humidair} . \qquad (2\text{-}10)$$

The mass flow rate of the condensed water is then used to determine the quantity of latent heating (h_{fg}) within the heat exchangers,

$$\dot{Q}_{LatentHeat} = \dot{m}_{condensedwater} h_{fg} . \qquad (2\text{-}11)$$

CAES Simulator's Saturation_Data_T function is called to interpolate h_{fg} from the water properties table. If condensation does not occur the latent heat is set to zero. The heat of condensation is then added to the convective heat transfer,

$$\dot{Q}_{Total} = \dot{m} c_p (\Delta T) + \dot{Q}_{LatentHeat} \qquad (2\text{-}12)$$

to find the total heat extracted during cooling, where ΔT is the temperature difference between the air entering and exiting the heat exchanger.

2.2.4 Compression Cycle Computational Model

CAES Simulator utilizes a finite differencing scheme to discretize the mass flow rate over the compression cycles. Boundary conditions are user defined and include temperature, pressure and humidity at the entrance and exit of each stage. The high pressure (HP) compressor cycle steps through a time iterative loop until the pressure within the tank reaches its upper limit. The term air storage and tank will be synonymous throughout this text. The low pressure (LP) cycle is governed by the flow rates determined by the HP compressor flow rates. CAES Simulator assumes that the power supplied to the HP compressor is constant and the flow rate varies according to the pressure ratio between the HP compressor inlet and tank pressure. Thermodynamic properties for humid air are calculated prior to each compression cycle. Refer to Section 2.3.2.

The HP compressor computational cycle first initializes the pressure ratio (r), mass flow rate ($\dot{m}$), mass of the tank (m_{tank}), temperature at the exit (T_{exit}), and the compressor polytropic coefficient (γ). Values for the inlet temperature (T_{inlet}), inlet pressure (P_{inlet}), compressor work input and the lower limit tank pressure (P_{TankLL}) are defined by the user. The initial pressure ratio between the compressor inlet and exit is defined as,

$$r = \frac{P_{TankLL}}{P_{inlet}}. \qquad (2\text{-}13)$$

Mass flow rates are found assuming constant power (W_{in}) using the relation,

$$\dot{m} = \frac{W_{in}}{\left(\frac{\gamma R T_{inlet}}{\gamma - 1} \left[r^{\frac{\gamma - 1}{\gamma}} - 1 \right] \right)}. \qquad (2\text{-}13)$$

The initial mass of humid air in the storage tank is found using the ideal gas equation with the user defined initial tank temperature (T_{Tank}). The air temperature leaving the compressor is found using the polytropic relation,

$$T_{exit} = T_{inlet} r^{\frac{\gamma - 1}{\gamma}}. \qquad (2\text{-}14)$$

The polytropic coefficient (γ) is found using the compressor adiabatic efficiencies (η_C), defined by the user, by comparing the polytropic work to the isentropic work with the relation,

$$\eta_C = \frac{\frac{\gamma}{\gamma - 1}\left(r^{\frac{\gamma - 1}{\gamma}} - 1 \right)}{\frac{k}{k - 1}\left(r^{\frac{k - 1}{k}} - 1 \right)}. \qquad (2\text{-}15)$$

The reader can obtain a complete derivation of the previous equations in the referenced text [9-11].

The HP compressor is modeled using a forward differencing sequence, within a computational loop, that is programmed to exit when the pressure in the tank reaches a user defined value. Mass of the air within the storage vessel is found by discretizing the mass flow rate to find the mass of the air entering the tank,

$$m(n+1) = m(n) + \dot{m}(n)\Delta t \qquad (2\text{-}17)$$

where n represents the time step counter and Δt is the time step.[3] Applying a mass energy balance, the mass flow rate is then used to find the new tank temperature.

$$T(n+1) = \frac{(T_{in}\dot{m}k\Delta t + T(n)m(n))}{m(n) + \dot{m}\Delta t} \qquad (2\text{-}18)$$

Using a discretized time iterative version of the ideal gas law, the computational model calculates the pressure within the tank as,

$$P(n+1) = \frac{m(n+1)RT(n+1)}{Volume}. \qquad (2\text{-}19)$$

P_{Tank} is then used to find the new pressure ratio,

$$r = \frac{P(n+1)}{P_{inlet}} \qquad (2\text{-}20)$$

mass flow rate,

$$\dot{m}(n+1) = \frac{W_{in}}{\left(\frac{\gamma RT_{inlet}(n)}{\gamma - 1}\left[r(n+1)^{\frac{\gamma-1}{\gamma}} - 1\right]\right)} \qquad (2\text{-}21)$$

and exit temperature,

$$T_{exit}(n+1) = T_{inlet}(n) r(n+1)^{\frac{\gamma-1}{\gamma}} \qquad (2\text{-}22)$$

in iterative form.

After the mass flow rates at each time step have been determined from the HP cycle, CAES Simulator begins the LP cycle. The computational model begins by calculating the physical properties of the ambient air at the user defined humidity, pressure and temperature. CAES Simulator then applies the flow rates and air properties into (eq. 2-22) to find the exit temperature and calculates the required compressor work input as,

$$W_{in}(n) = \left(\frac{\dot{m}(n)\gamma R T_{Ambient}}{\gamma - 1} \left[r^{\frac{\gamma-1}{\gamma}} - 1 \right] \right) \qquad (2\text{-}23)$$

where r is held constant as the ratio between the first stage heat exchanger and the ambient air pressure.

2.2.5 Expansion Cycle Computational Model

Similar to the compression cycles, the expansion cycle utilizes a forward finite differencing scheme to discretize the mass flow rate over the expansion cycles. The high pressure expander cycle steps through a time iterative loop until the pressure within the tank reaches its lower limit. The flow rates in the low pressure cycle are determined by the flow rates in the HP expander cycle. Power supplied by the LP turbine is assumed constant and the flow rate varies according to the pressure ratio between the tank pressure

and the HP expander exit. Thermodynamic properties for humid air are calculated prior to each expansion cycle. Refer to section 2.3.3.

Initializations for the HP expansion cycle are taken from the user defined boundary conditions. Equipment limitations on temperature and pressure govern the operational conditions of the system. The user defines the temperature at the inlet of the HP expander, the upper pressure limit of the tank, work output and exit pressure of the HP expander. Beginning with the pressure ratio, the HP expansion cycle is initialized by calculating the polytropic coefficient (eq. 2-16), mass flow rate,

$$\dot{m} = \frac{W_{out}}{\left(\frac{\gamma R T_{inlet}}{\gamma - 1} \left[1 - r^{\frac{\gamma - 1}{\gamma}} \right] \right)} \qquad (2\text{-}24)$$

mass in the tank (eq.2-19) and exit temperature (eq. 2-22) at the start time of the cycle respectively.

The HP expander cycle operates by discretizing the mass flow rate equation to find the mass of the air left within the tank as time passes,

$$m(n+1) = m(n) - \dot{m}(n)\Delta t \,. \qquad (2\text{-}25)$$

As air escapes from the storage tank the internal pressure decreases isentropically. Applying a mass energy balance (Eq 2.1), the mass flow rate is then used to find the new tank temperature,

$$T(n+1) = \frac{(T(n)m(n) - T_{in}\dot{m}k\Delta t)}{m(n+1)} \,. \qquad (2\text{-}26)$$

The expansion cycle then proceeds to find the pressure ratio and the mass flow rate,

$$\dot{m} = \frac{W_{out}}{\left(\frac{\gamma R T_{inlet}}{\gamma - 1} \left[1 - r(n+1)^{\frac{\gamma-1}{\gamma}} \right] \right)} \qquad (2\text{-}27)$$

where the inlet temperature is held constant at the first stage regenerator exit temperature. The next time step tank temperature (Eq. 2-26) and the HP expander exit temperature (eq. 2-22) are then calculated.

Similar to the compression process, the HP and LP expansion cycles are in series and have the same flow rates. After the flow rates are determined from the HP expansion cycle the LP cycle determines the power supplied by the LP expander,

$$\dot{W}_{out}(n) = \left(\frac{\dot{m}(n) \gamma R T_{Inlet}}{\gamma - 1} \left[1 - r^{\frac{\gamma-1}{\gamma}} \right] \right) \qquad (2\text{-}28)$$

where the inlet temperature is held constant at the second stage regenerator exit temperature.

2.2.6 Heat Transfer and Condensation During Expansion Cycle

Thermal energy from the compression cycle is recuperated by heating the compressed air before it is sent to the expander using a regenerator. This aids with expansion and raises the overall efficiency of the plant. A heat exchanger transfers thermal energy to the air before each stage of expansion. Air passing through the

turbine is cooled during the process of expansion allowing for the possibility of condensation. The heat exchanger calculations of the Expansion Cycle serve two main functions. CAES Simulator calculates the required heating load for power production and performs a condensation check after each expansion cycle. This information is then used to find the psychometric properties of the air before it is used to generate power in the low pressure turbine.

Similar to the heat exchanger condensation checks during compression, CAES Simulator analyzes the psychometric properties of the air to find the humidity ratio and heat capacity of the air. After the first stage turbine the partial pressure of water vapor is calculated using a modified version of Eq. 2-8 as,

$$P_v = \frac{\omega P_{LP}}{\omega + .622} \qquad (2\text{-}29)$$

where P_{LP} is the pressure of the air entering the low pressure turbine. P_v is then sent to the subprogram Saturation_Data_T which determines the wet bulb temperature using the methods described in Section 2.3.3. Saturation_Data_T then compares the exit air temperature of the high pressure turbine to determine if latent heat is lost to the system. If the exit temperature of the turbine at any point in time during the expansion cycle is less than the saturation temperature for P_{LP} the program displays a warning and proceeds to calculate the new absolute humidity using Eq 2-8. The model then calculates the thermodynamic properties using the methods described in Section 2.3.2.

The expansion cycle must also ensure that the heat exchanger does not supply more energy than is extracted during the compression cycle. The discretized HP Turbine loop continually compares the energy collected during compression to the sum of the heat

exchanged during each time step. If the loop determines that the heat exchanger has exceeded its capacity to continue heating the air, the user is prompted with an error message. To achieve adiabatic conditions the user must then run the simulation with reconfigured boundary conditions such as generated loads and turbine inlet temperatures. Simulated data can still be acquired for a nonadiabatic system allowing the user to model CAES systems with an external heat source.

It should be noted that the design of a thermal energy storage system used for an AA-CAES is beyond the scope of this study. CAES Simulator does not attempt to analyze the performance of a thermal energy storage system. Thermal energy stored and transferred during the heat exchanger cycle is assumed isentropic with no losses to the surroundings. Overall plant efficiency calculated using CAES Simulator does not include the efficiency of the thermal energy storage system (TES). TES efficiency will be dependent on the design of the TES and heat exchangers.

2.3 Graphical User Interface Computational Model

2.3.1 Computational Model Software Package

The analysis of the an adiabatic compressed air energy storage system was facilitated by the development of a simulation program coded using the commercial software package Matlab©. Using a graphical user interface (GUI) the user is prompted to enter parameters such as temperatures and pressures that control the simulation. The software allows the user to run a simulated CAES system and collect analytical data such as plant efficiency. The simulation program is comprised of a main GUI titled “CAES

Viewer" and subprograms "CAES Simulator", "CAES Variables" and "CAES Schematic". See Figure 2-1 for a flow chart of the main GUI figures.

CAES Viewer's two main functions are to display data and call subprograms. It allows the user to toggle between data sets for the compressors and expanders. After acquiring data from CAES Simulator, data are listed and plotted on the CAES Viewer GUI. Eight plots display time series data for:

- Temperatures, pressures and mass of air within the air storage
- Heat exchanged within the High Pressure (HP) and Low Pressure (LP) heat exchangers
- Mass flow rates, pressure ratios and exit temperatures of the HP compressor and HP turbine

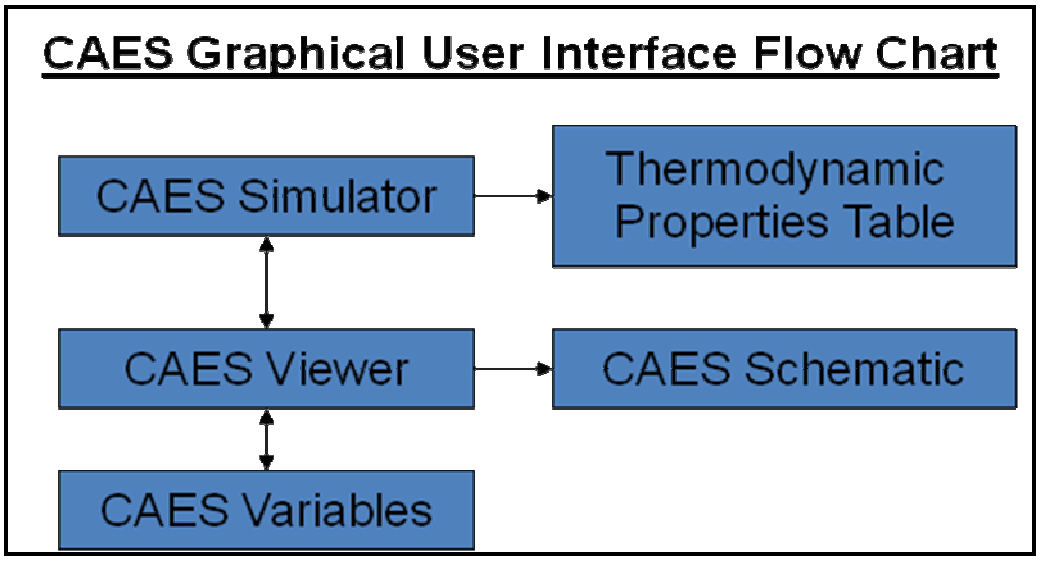

Figure 2-1 Flow chart of the main graphical user interface contained in the CAES simulation package.

Displayed data can be saved as a Matlab workspace '.m' file, exported to an Excel spreadsheet, or exported as a comma separated variable file. A text box displays important parameters such as plant efficiency, run times and energy capacity. CAES Viewer also contains control buttons that call other subprograms to run the simulation and display the data on a schematic. Refer to the flow chart in Figures 2-1 and 2-2 describing the details of CAES Viewer and see Figure 2-3 for a screen shot of CAES Viewer.

CAES Simulator performs system calculations for three main processes which include the compression cycle, expansion cycle and heat exchange process. Using a time iterative discretization method CAES Simulator receives data from CAES Viewer and returns the processed data. All calculations for the compressed air system are performed in the CAES Simulator. The CAES Simulator is also programmed with the capability of calling and collecting data from a thermodynamic property library for water which is used to identify the psychometric properties of humid air. Refer to Section 2.3 for a detailed description of the calculations used to model the cycle, along with Appendix A which contains code for CAES Simulator.

The CAES Simulator is controlled by the user defined boundary conditions and equipment limits applied using CAES Variables. The user can select an infinite number of equipment configurations by inputting the mechanical and thermodynamic limits of each component of the CAES system. Another major strength of the CAES Simulator is its capacity to define ambient conditions within CAES Viewer allowing the user to simulate environmental conditions at a potential location such as the proposed site in

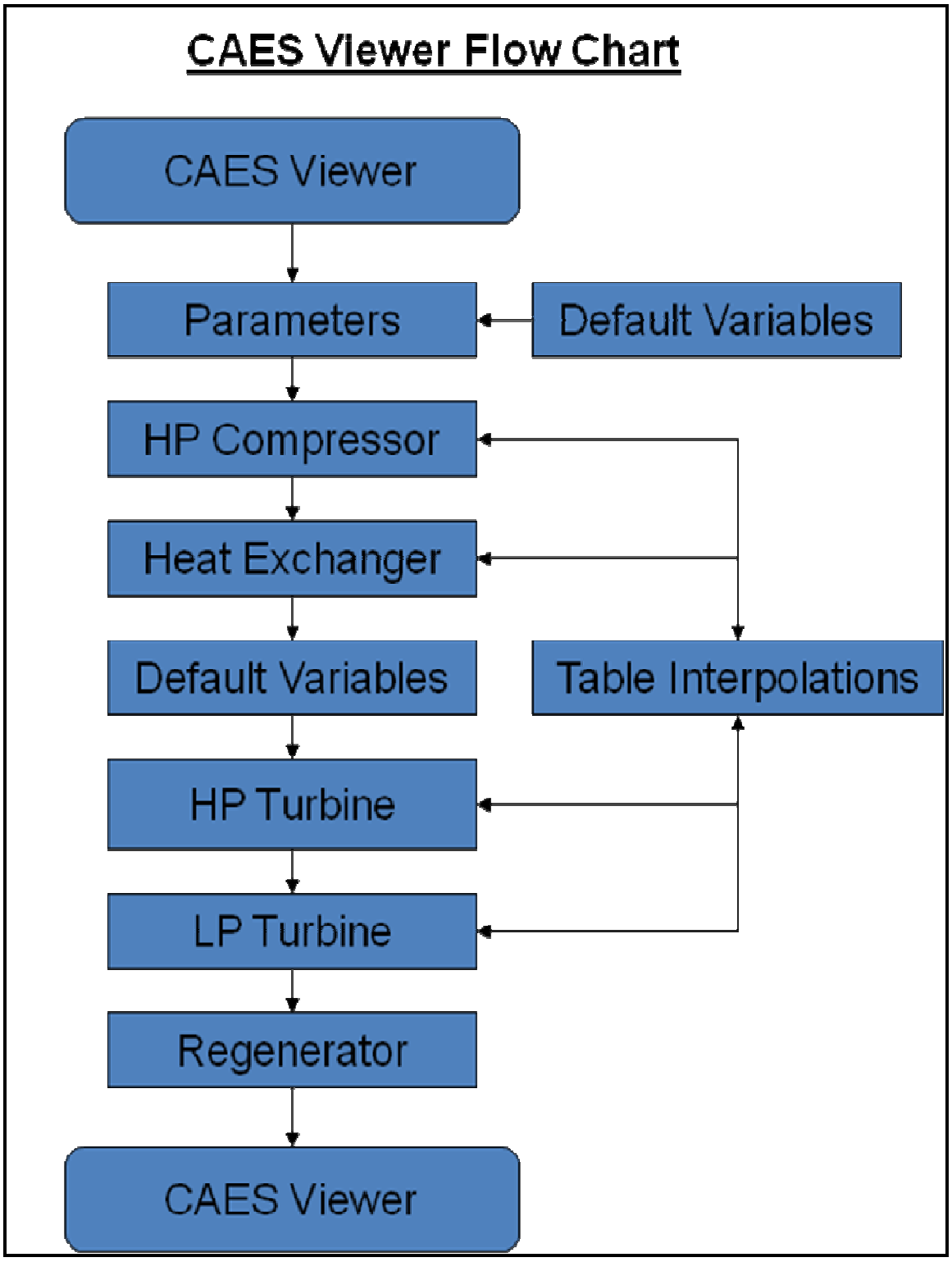

Figure 2-2 Flow chart of the subprograms used in CAES simulator.

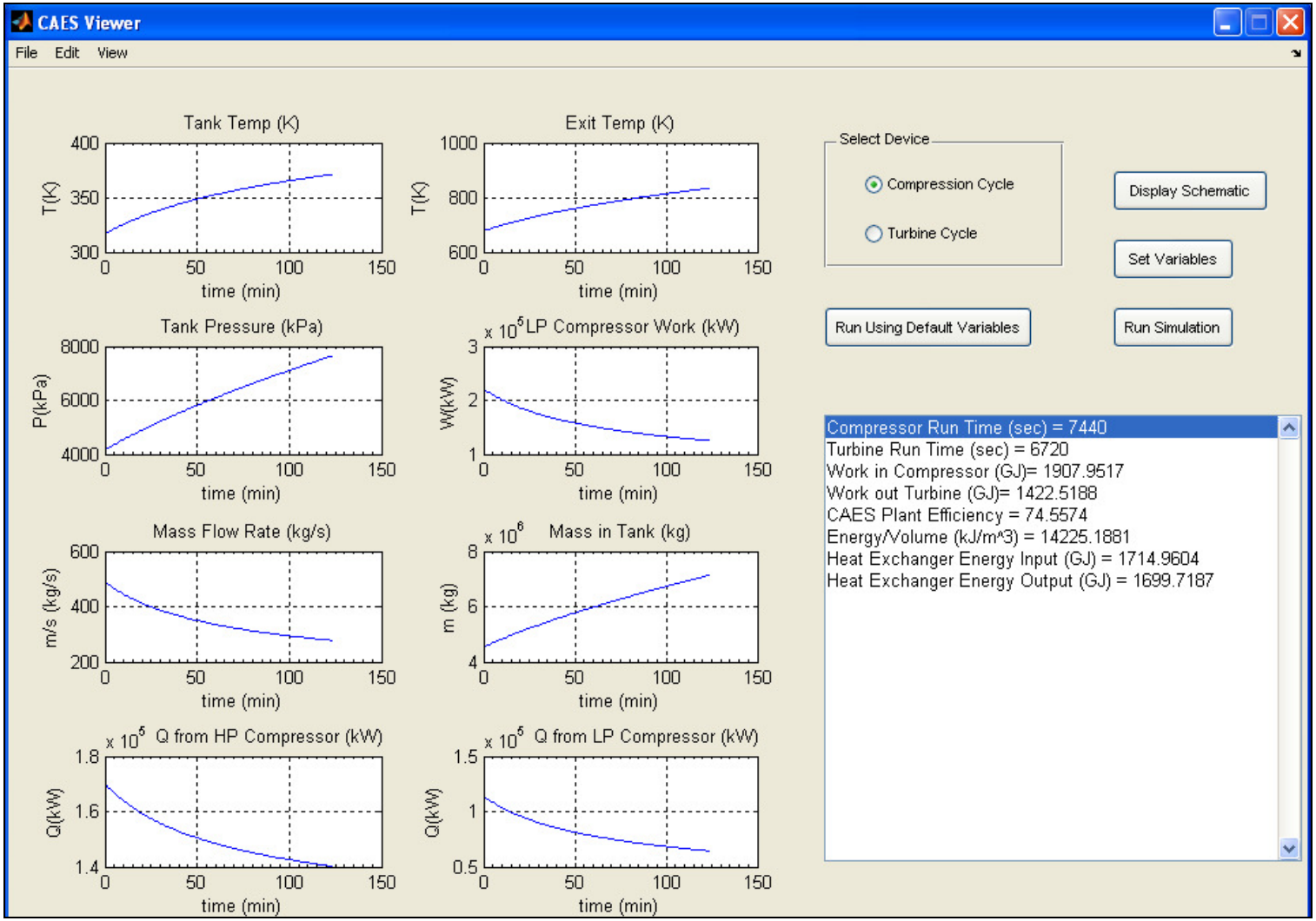

Figure 2-3 Screen shot of CAES Viewer graphical user interface.

Cottonwood Canyon, Utah. CAES Viewer's display is divided into five categories, separating input fields pertaining to the physical characteristics of the potential plant, ambient conditions and equipment properties. See Figure 2-4 for a screen shot of CAES Variables. CAES Variables is called by the Set Variables button displayed on the CAES Viewer GUI and is pre-programmed with default variables which were originally used as a reference for programming purposes.

The CAES simulation package also contains a graphical display of the results obtained from the simulation. CAES Schematic receives data from CAES Viewer and displays system properties of the simulated data on a schematic of the overall plant. The subprogram was added as a convenient way for the user to display a broad overview of the functionality of the system. These properties include power production, plant efficiency, and temperature and pressure limits. See Figure 2-5 for a screen shot of CAES Schematic.

2.4 Review

This chapter described the development of a compressed air energy storage computational model. The simulation software package, CAES Simulator, was developed to allow the user to input parameters allowing for the modeling of a variety of configurations of an AA-CAES plant. Conservation equations for transient flow along with appropriate equations of state were used to computationally model an AA-CAES plant that uses humid ambient air to store electrical power. The model utilizes a forward differencing method to calculate time iterate parameters within the system. A major benefit of the model is its capability of adapting to changing psychometric properties in

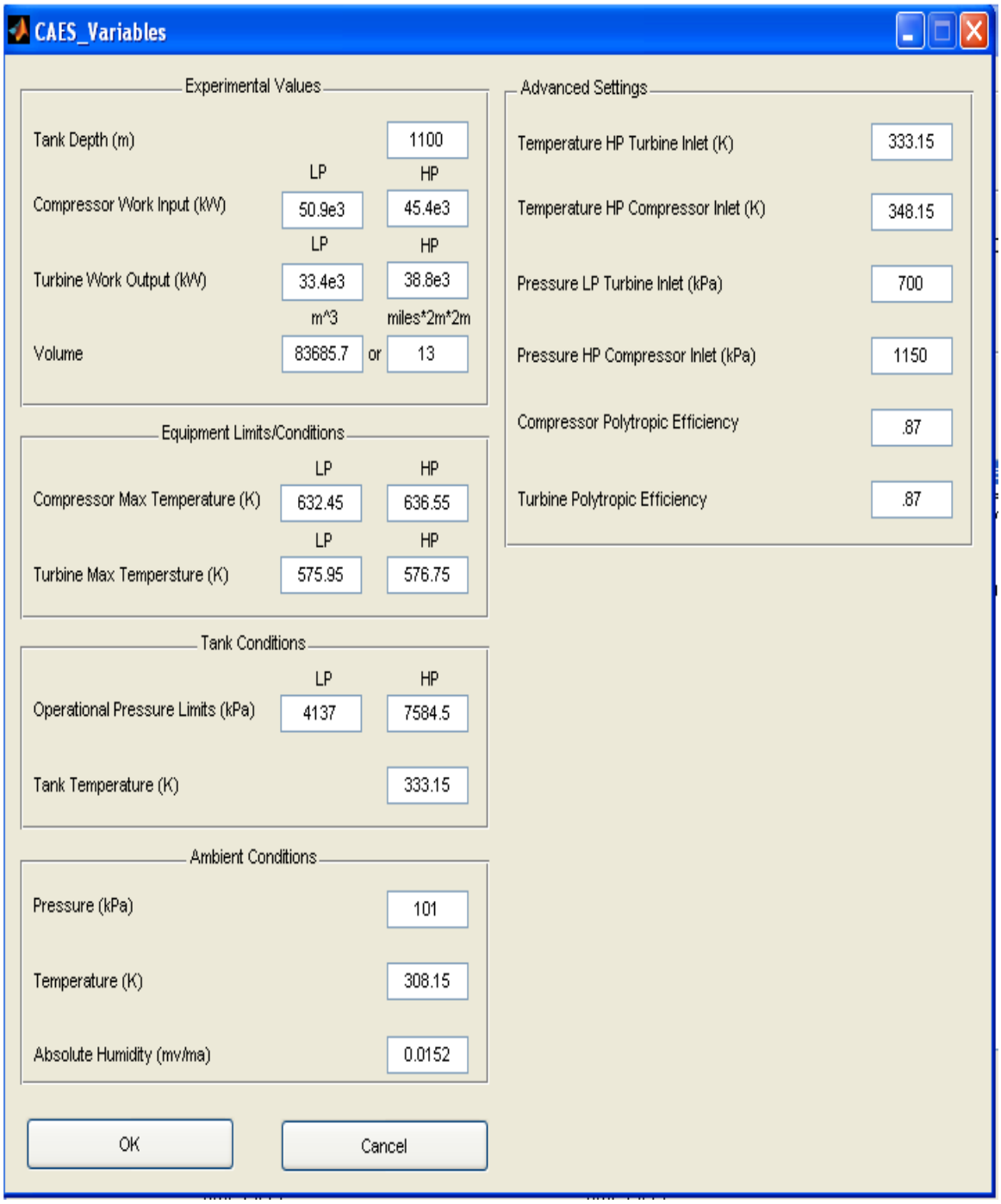

Figure 2-4 Screen shot of the parameter input GUI CAES Viewer.

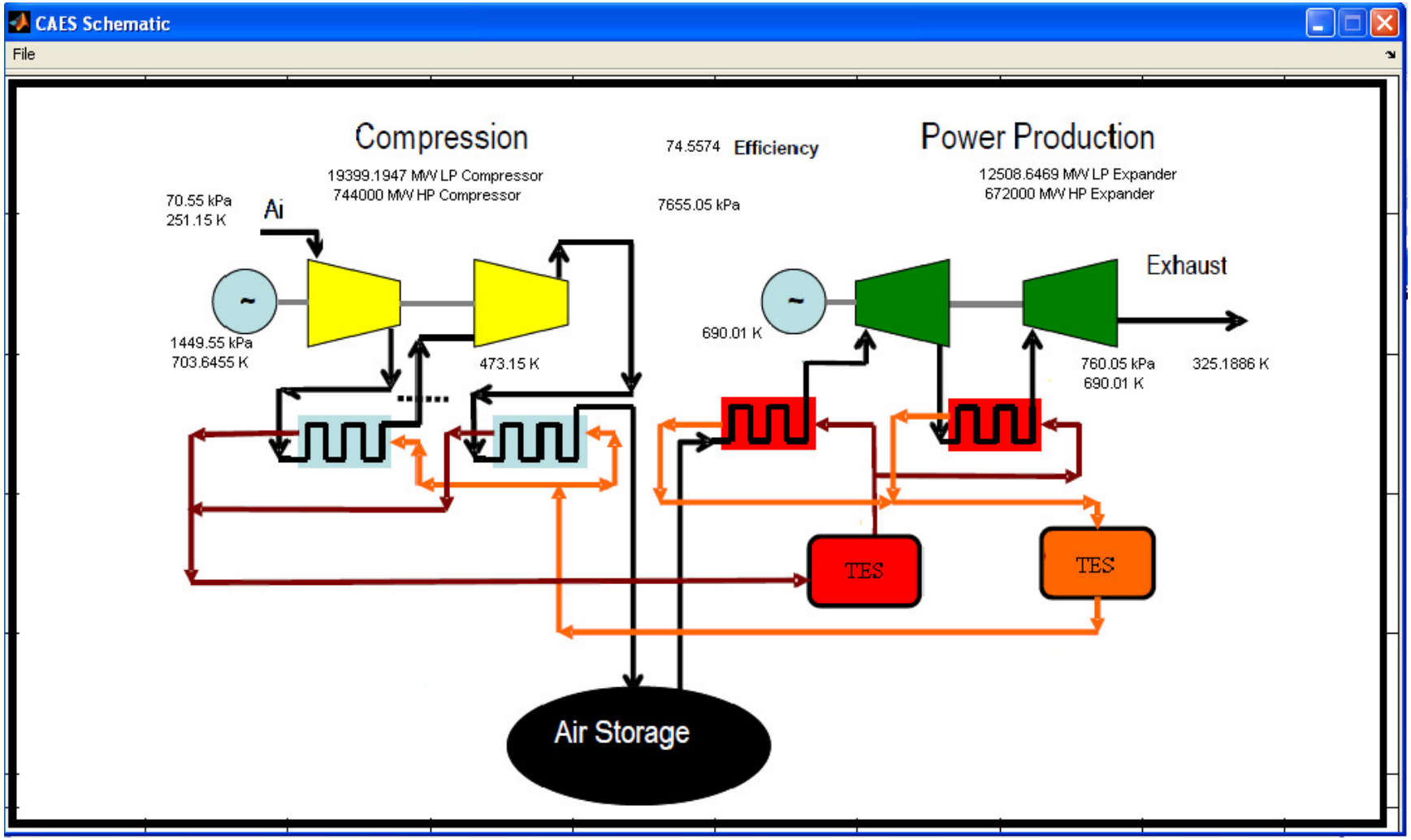

Figure 2-5 Screen shot of the graphical display GUI CAES Schematic.

the case of condensation and latent heating. In the following chapter an experimental study of the operation of a compression cycle will validate the accuracy of the computational model.

CHAPTER 3

EXPERIMENTAL PROCEDURE

3.1 Overview

CAES Simulator was tested against experiment data to ensure the code's validity before performing a feasibility study. CAES Simulator's computational models deviation from experimental data must be quantified before the computational results may be used for this feasibility study. Experimental data of a two stage compression cycle were generated using a 280 HP compressor residing on the 1st floor of the Merrill Engineering building located at the University of Utah. The computational model was used to simulate the two stage compression cycle and a comparison study of the results was conducted to verify the validity of CAES Simulator's model. It should be noted that the turbine generation cycle is not included in this validation study. This chapter describes the experimental apparatus and the methods used to obtain results.

3.2 Experimental Setup

3.2.1 Experimental Apparatus

A Gardner-Denver tandem horizontal two stage compressor model RL 1155CB was used to charge a 8.5 m^3 tank up to 9.6 kPa (see Figure 3-1). Attached to a supersonic wind tunnel, the tank is used to rapidly discharge air to the flow chamber. Air enters the system from inside the Merrill Engineering Building and is conditioned by the building's HVAC System. Compression occurs at two stages with heat removal after each stage. A shell and tube heat exchanger cools the air leaving the first stage. The air is then

Figure 3-1 Gardener-Denver tandem horizontal two-stage compressor model RL 1155CB.

compressed in the second stage compressor and enters a second stage heat exchanger. After compression, cooling oil is separated from the air using an oil separator and then the air is dehumidified using a desiccant dryer tank. A snubber tank removes pressure transients from the fluid before the air is stored in the main tank.

3.2.2 Data Logging and Sensing Equipment

Using data logging and sensor equipment experimental data were obtained at various positions within the compressor. Refer to Table 3-1 for specifics. Six Type T thermocouples were used to acquire temperature readings. Refer to Figure 3-2 for a schematic of the pressure and temperature reading positions. Temperature readings were taken at:

- 1st Stage compressor outlet (T1)
- 2nd Stage compressor inlet and outlet (T2 and T3)
- Heat exchanger inlet and outlet (T4 and T5)
- Compressor intake (T6)

Temperature readings were logged using an Omega Logger OM-3000.

Transient pressure readings were logged using a HOBO© Energy Logger Pro™. Three Ashcroft pressure transducers, two rated 0-200 psig and one rated 0-100 psig were used to obtain pressure data. A Setra pressure transducer, rated 10.0 in. WC, was used for flow measurements by taking pressure readings across the orifice plate. Pressure readings were taken at the:

- Nozzle orifice plate (P1)
- 2nd Stage compressor inlet (P2)
- 2nd Stage compressor outlet (P3)

Table 3-1 Temperature and pressure sensor placement.

Temperature (#)	*Pressure (#)*	*Location*
	P1	Orifice Plate
T1	P2	Compressed air after 1st stage compression
T2		Cooled compressed air after 1st stage compression
T3	P3	Compressed air after 2nd stage compression
T4		Cooling water inlet
T5		Cooling water outlet
T6		Ambient air
	P4	Compressed air in tank

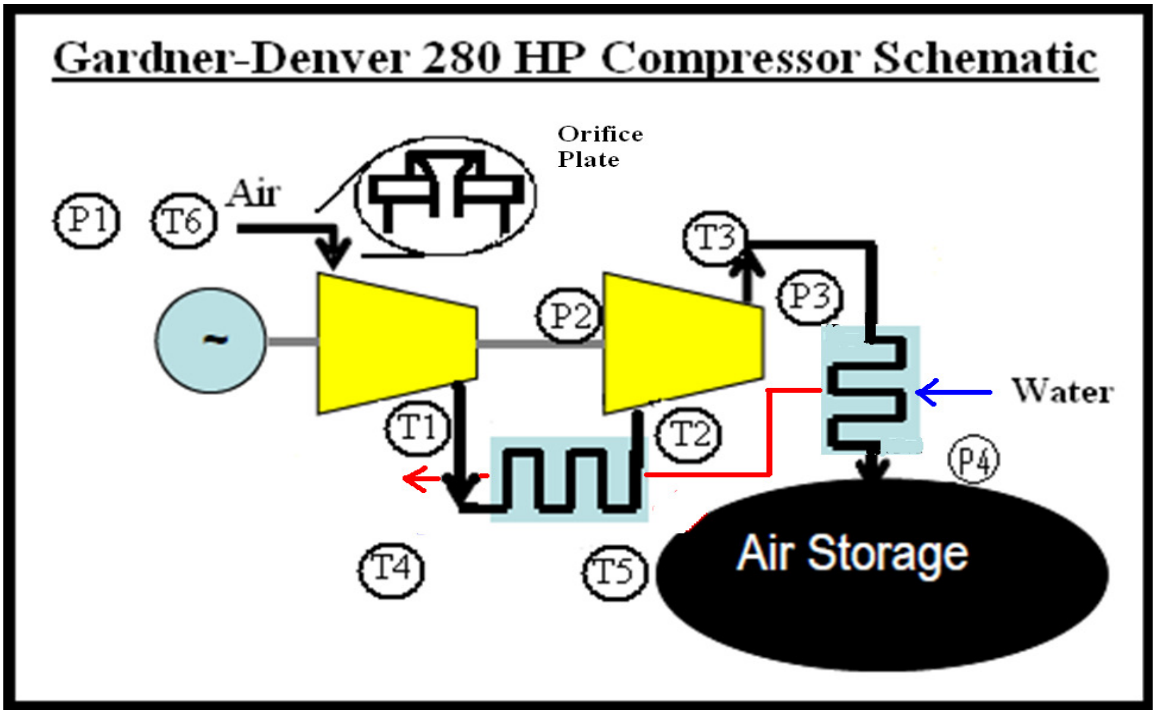

Figure 3-2 Gardner-Denver compressor schematic.

- Storage Tank (P4)

Along with the pressure and temperature data, power readings were logged as the compressor filled the tank. Power readings were taken using a Fluke Power Logger model 1735 at the breaker panel that supplies electricity to the compressor including its control system. The additional electric loads on the compressor from automatic safety and purge valves were assumed to be insignificant and were not accounted for in the final analysis. The psychometric conditions of the ambient air are a major component of this analysis. A Taylor model 1330PJ red spirit filled sling psychrometer was used to measure dry bulb and wet bulb temperatures before and after each experiment. Humidity ratio was obtained by finding the saturated pressure using the Hyland and Wexler equation [12],

$$\ln P_v = \sum_{i=-1}^{3} C_i T^i + C_4 \ln T \qquad (3.1)$$

where T is the wet bulb temperature in Celsius, and applying it to equation (2-7). Coefficients are given in Table 3-2. Barometric pressure was also obtained using a barometer.

3.2.3 Heat Exchange Measurements

A tube and shell heat exchanger removes waste heat from the 1st stage compressed air before the air is compressed in the 2nd stage compressor. A sight glass rotameter was used to measure the cooling water transferred through the heat exchanger. Water is received from the building's supply and discharged as waste water to the sewage

Table 3-2 Hyland and Wexler's saturation pressure equation coefficients.

Coefficient	*Value*
C_{-1}	-0.58002206E+4
C_0	0.13914993E+1
C_1	-0.48640239E-1
C_2	0.41764768E-4
C_3	-0.14452093E-7
C_4	0.65459673E+0

system. The water is not recycled through the heat exchanger. Air traveled through the shell side of the heat exchanger and lost thermal energy to the surrounding room air and cooling water passing through the tubes of the heat exchanger. Heat exchanged in the intercoolers was calculated using an energy balance,

$$q = \dot{m}_{H2O} c_{pH2O} (T_3 - T_2) \qquad (3.2)$$

where T_3 and T_2 were measured after the first stage heat exchanger and compressor, respectively, $\dot{m}_{H20}$ is the mass flow rate of the cooling water and c_{pH2O} is the specific heat of the cooling water.

3.2.4 Air Mass Flow Rate Measurements

A nozzle orifice plate was used to measure the air mass flow rate at the inlet of the compressor. See Figure 3-3 for the experimental setup. Following the guidelines detailed in ASME MFC-3M-1989[13] the flow was measured using a 50.8 mm diameter brass nozzle. The plate was placed at the end of a 1.8 m pipe with the inlet side open to the atmosphere. A pressure transducer was placed 82.6 mm downstream of the plane of the inlet face of the nozzle in accordance with the ASME Standard. Pressure brass

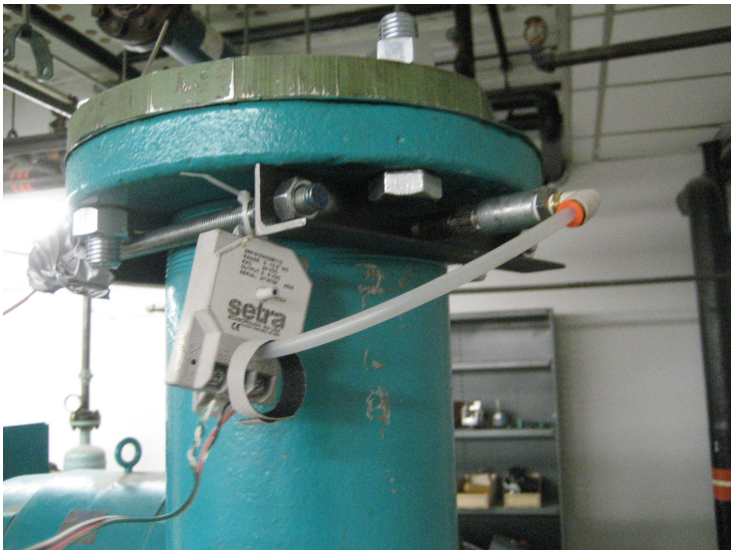

Figure 3-3 Orifice plate used to measure mass flow rates at the inlet of the compressor.

nozzle. The plate was placed at the end of a 1.8 m pipe with the inlet side open to the atmosphere. A pressure transducer was placed 82.6 mm downstream of the plane of the inlet face of the nozzle in accordance with the ASME Standard. Pressure measurements were obtained using pressure transducers as described in Section 3.2.1. Refer to Reference 13 for the derivation of the following five equations.

Mass flow rates ($\dot{m}$) were logged using the pressure differential between the tap and the atmospheric pressure with the relation,

$$\dot{m} = \frac{\pi}{4} C \varepsilon_2 d^2 \sqrt{\frac{2\Delta p \rho_{f_2}}{1-\beta^4}} \ . \tag{3.3}$$

The discharge coefficient was estimated as,

$$C = 0.9975 - 0.00653(10^6 \beta / \mathrm{Re})^{0.5} \tag{3.4}$$

where the Reynolds number is the ratio of dynamic to viscous forces or,

$$\mathrm{Re} = \frac{\rho V D}{\mu}. \tag{3.5}$$

β is a shape factor that relates the diameter of the nozzle (d) to the diameter of the inlet pipe (D) as,

$$\beta = d/D. \tag{3.6}$$

The expansion coefficient (ε_2) is calculated using,

$$\varepsilon_2 = (1 + \Delta p / p_2)^{0.5} \left[\left[\frac{k r^{\frac{2}{k}}}{k-1} \right] \left[\frac{1-\beta^4}{1-\beta^4 r^{\frac{2}{k}}} \right] \left[\frac{1-r^{\frac{k-1}{k}}}{1-r} \right] \right]^{0.5} \tag{3.7}$$

where k is the isentropic exponent and τ is the pressure ratio.

3.3 Equipment Calibration

Validation of the computational model requires precise measurements be taken at all points to ensure the accuracy of results. The thermocouples, rotameter and pressure transducers were calibrated to guarantee accurate and concise data. The following section outlines the measures used to calibrate these three pieces of equipment.

3.3.1 Thermocouple Calibration

Along with a psychrometer the six thermocouples were placed in an ice bath and brought to a constant temperature for five mins. Liquid water changes state to a solid at

0˚C at sea level. A mixture of water and ice was used to ensure a constant temperature allowing for calibration. The thermocouples were then removed from the ice bath and returned to room temperature. Temperature differences between the thermocouples and the psychomotor were within acceptable limits and fall within the limits of error determined by the manufacturer. A standard deviation for each thermocouple was calculated to determine the precision of the thermocouple readings at the temperature of the ice bath and the room temperature. The standard deviation of the thermocouples did not exceed 0.6˚C. See Table 3-3 for results of the calibration and Appendix B for the limits of error.

3.3.2 Rotameter Calibration

A site glass rotameter was placed in the cooling water stream of the heat exchanger. The site glass contained percentage markings of the measurable flow rate capacity of the meter. Flow rates were brought to 50% capacity and allowed to stabilize for approximately 3 min. The flow was then redirected into a five gallon bucket and filled for 1 min. The bucket was then weighed to measure the mass and volume of the water. Temperatures of the water were recorded to determine the density. This calibration test was run three times and the resulting mass flow rates were averaged. See Table 3-4 for results. Flow rates were consistent averaging 0.0113 kg/minute.

3.3.3 Pressure Transducer Calibration

An oil filled 160 psi Omega pressure gauge was connected to three Ashcroft pressure transducers and the storage tank. The tank was brought up to various pressures while each device measured the pressure in the tank. The test was repeated for the

Omega 10 in. WC pressure transducer using a bicycle pump and a 20 in. WC Omega pressure gauge. Pressure readings were within ±1.5 psi and ±.1 in. WC which is within an acceptable degree of accuracy for the conditions of this validation study. See Table 3-5 for results of the pressure calibration and the percent error each pressure transducer deviated from the pressure gauge used for calibration.

3.4 Comparison of Experimental and Computational Data

3.4.1 Experimental Conditions

Experimental results were obtained on a precipitous day when the absolute humidity reached 1.83E-2 g H_2O/g dry Air. The dry bulb and wet bulb temperature were 20.81˚C and 10.82˚C, respectively. Cooling water was pumped through the heat exchanger at a rate of 8.71E-02 g H_2O/g dry Air. The tank was pressurized from an atmospheric pressure of 85.99 kPa to 1205.76 kPa. Compressed air energy storage plants cycle between pressures well above atmospheric pressure. For this reason the data obtained during start up were not used. Experimental results were obtained for tank pressures that range between 781.69 kPa and 1205.76 kPa. Air pressure after the 1st stage compression was set at a constant 368.69 kPa. The belt driven compressor had a 55% mechanical efficiency losing a substantial amount of energy to friction.

Table 3-3 Thermocouple calibration results.

Thermocouple Calibration Results				
Termocouple #	Room Temperature (C)	Ice Bath Temperature (C)	Room Temp Standard Deviation (C)	Ice Bath Temp Standard Deviation (C)
T1	22.3	0.8	0.2	-0.3
T2	22.8	0.5	-0.3	0
T3	22.6	0.8	-0.1	-0.3
T4	22.9	0.5	-0.4	0
T5	22.9	1.1	-0.4	-0.6
T6	22.4	0.9	0.1	-0.4
Pyscrometer	22.5	0.5	0	0

Table 3-4 Cooling water mass flow rate calibration.

Mass Flow Rate Calibration Results				
Test	Mass Bucket (kg)	MassWater (kg)*	Temperature (deg C)**	Flow Rate (m^3/min)
1	11.45	11.45	20.8	0.01145
2	11.1	11.1	21.1	0.0111
3	11.35	11.35	21.4	0.01135
			Average	0.0113
*Mass Empty Bucket (kg) = 0.85				
**Density of Water (kg/m3) = 1000 for temperatures between 20-25 C.				

Table 3-5 Pressure transducer calibration.

Pressure Transducer Calibration Results						
Pressure Gauge (psi)	25	% Error	50	% Error	75	% Error
P2	26.124	4.50	50.96	1.92	75.75	1.00
P3	25.235	3.40	50.125	1.64	75.056	0.92
P4	25.896	2.62	50.556	0.86	75.512	0.61
Pressure Gauge (in. WC)	**2.6**	**% Error**	**5.3**	**% Error**	**7.5**	**% Error**
P1	2.609	0.35	5.355	1.04	7.523	0.31

3.4.2 Pressure Data Comparison

This validation study will began by comparing the computational and experimental pressures. CAES Simulator assumes pressurized air is released directly into the tank without passing through a heat exchanger or deliquescent drying. Air entering the storage tank from the compressor experiences a pressure drop from forcing mechanical check valves open. It is also cooled by sensible and latent heat exchange as it passes through the heat exchanger and dryer tank, reducing the pressure of the air. Figure 3-4 displays the pressure of the air after 2nd stage compression and the tank. The pressure drop changes as the air increases in pressure and the dryer tank media becomes saturated. Conditions leading to the pressure drop are outside the scope of this study and were not

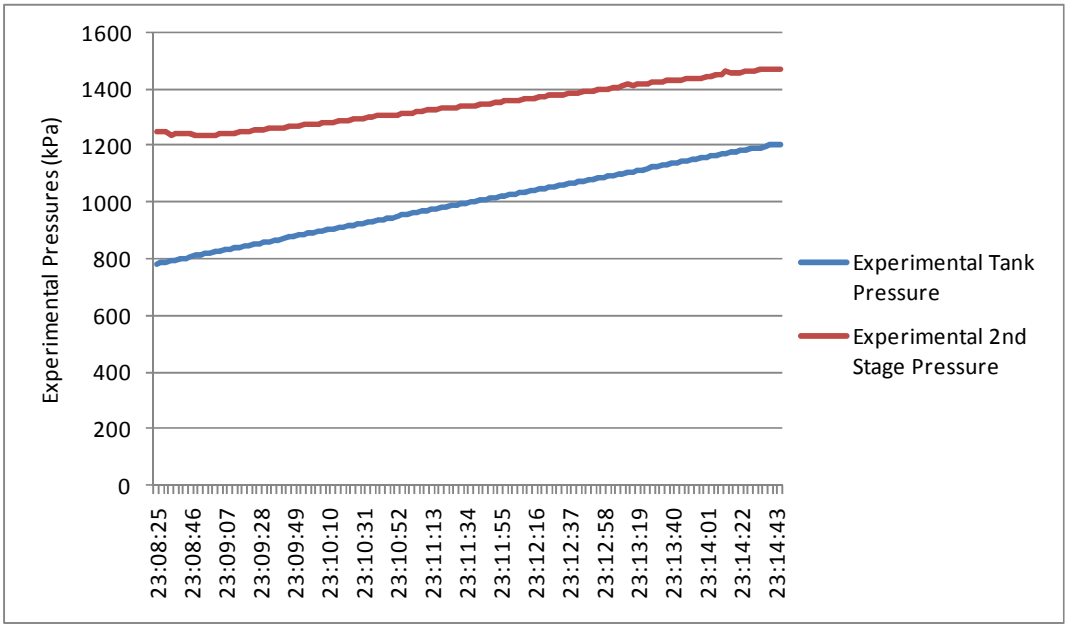

Figure 3-4 2nd stage and tank air pressure as it changes in time.

modeled explicitly. The following method describes techniques used to quantify the drop in pressure.

Pressure limits were used to control time iterative loops for the compression cycle. The HP compression cycle loop assumes the tank pressure increases at the same rate as the HP compressor exit pressure. To account for the pressure loss between the compressor and tank, an equation was obtained by applying linear regression to the pressure difference and 2nd stage exit pressure. The computational model was modified to calculate the 2nd stage exit pressure (P_{Exit}) from the tank pressure (P_{Tank}), assuming a pressure drop across the mechanical check valve between the compressor and tank (ΔP) represented as,

$$\Delta P = -0.4011(P_{Exit}(kPa) / P_{Tank}(kPa)) * P_{Tank} + 746.15(kPa). \qquad (3.8)$$

Tank pressure was used to control the time iterative loop by stepping out of the sequence when the tank pressure reached its upper limit. Figure 3-5 and Figure 3-6 display the experimental and computational results of the tank and 2nd stage pressures. As expected the computational pressures coincide with the experimental data with less than 1% difference.

3.4.3 Temperature Data Comparison

Computational temperature data were heavily dependent on the polytropic efficiency of the compressor. Polytropic efficiencies are governed by heat transfer during compression and must be found experimentally. Heat was lost by convection to the surroundings and by heat transferred to oil used to cool the compressor during both

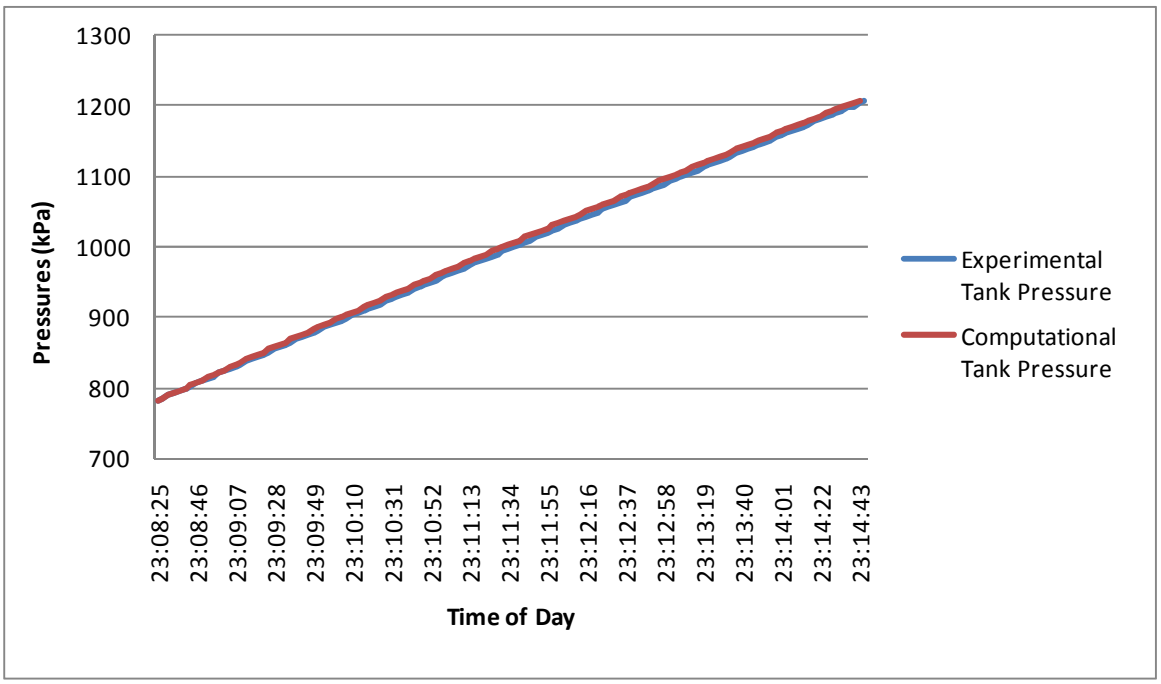

Figure 3-5 Experimental and computational results of the temporal pressure conditions in the tank.

phases of compression. Experimental polytropic coefficients (γ) were determined by comparing the pressure ratio across the inlet and outlet of the 1st and 2nd stage compressor to the temperature ratio (T_{Exit}/T_{Inlet}) by manipulating equation 2.21 as,

$$\gamma = \left(1 - \log_r \left(T_{Exit} / T_{Inlet}\right)\right)^{-1} \qquad (3.9)$$

Figure 3-7 displays the polytropic coefficients of the compression cycles. Irreversibilities during 1st stage compression were significantly less than those of the 2nd stage. Second Stage compression was nearly isothermal.

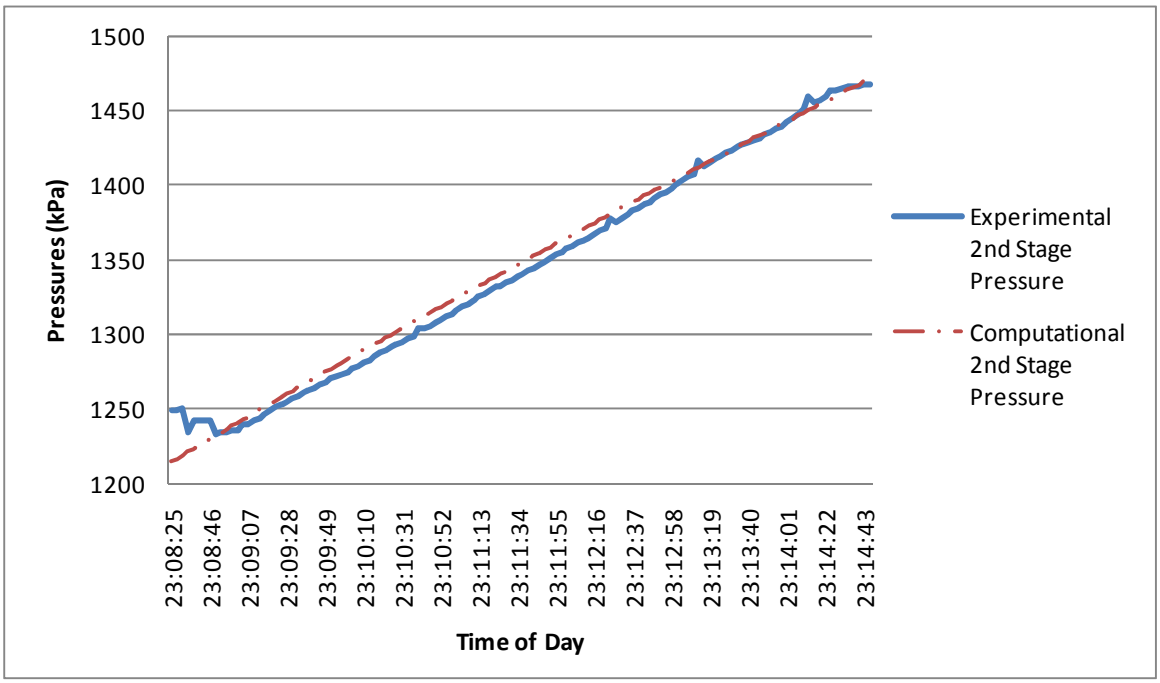

Figure 3-6 Experimental and computational results of the temporal pressure conditions after 2nd Stage compression.

CAES Simulator assumes constant polytropic efficiencies during compression cycles. The computational model was modified to account for the changing polytropic coefficients by calculating a trend line equation, from experimental polytropic coefficient data, using linear regression as,

$$\gamma = 7E-5*t+1.258 \qquad (3.10)$$

for the 1st stage and

$$\gamma = -0.0002*t+1.0977 \qquad (3.11)$$

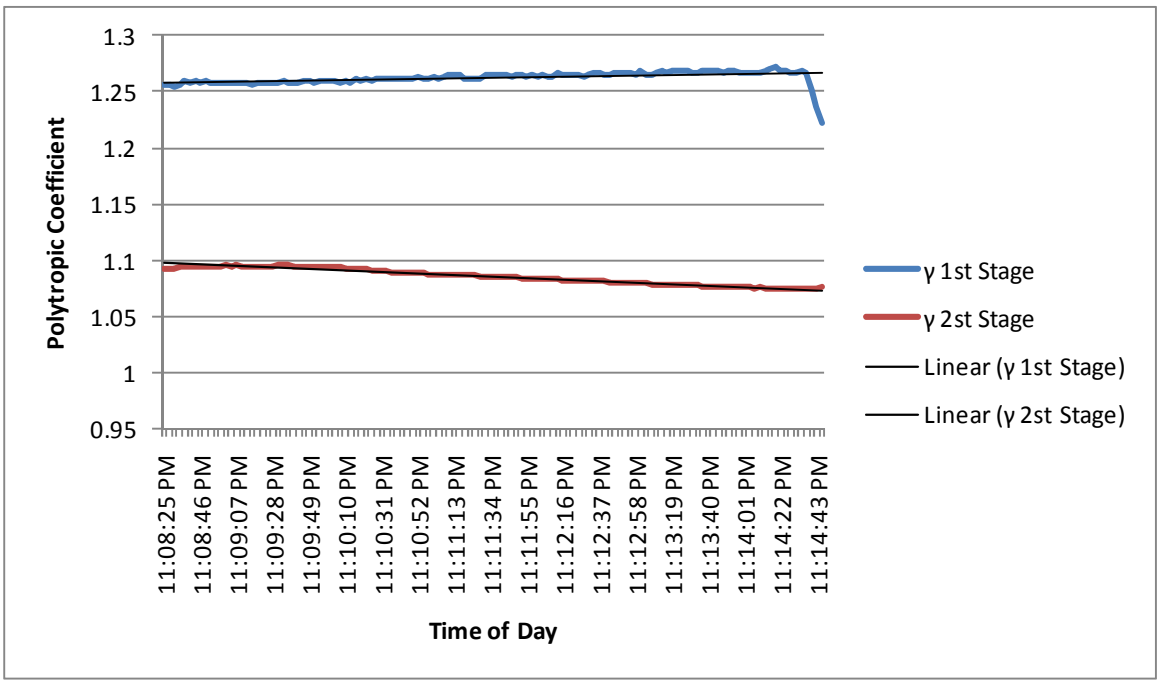

Figure 3-7 Experimental polytropic coefficients of the1st and 2nd stage compression including a linear regression trend line.

for the 2nd stage. Polytropic coefficients were calculated during each time step.

CAES also assumes the air temperature after the first stage heat exchanger is constant. Cooling water is first heated by the 2nd stage heat exchanger. The 1st stage heat exchanger's ability to collect heat is reduced as the entering cooling water's temperature rises. Using the same techniques described for γ, a trend line equation was applied to the air exiting the 1st stage heat exchanger and is defined as,

$$T_3 = 4.75\text{E-}7(K/s)*t+307.72(K). \qquad (3.12)$$

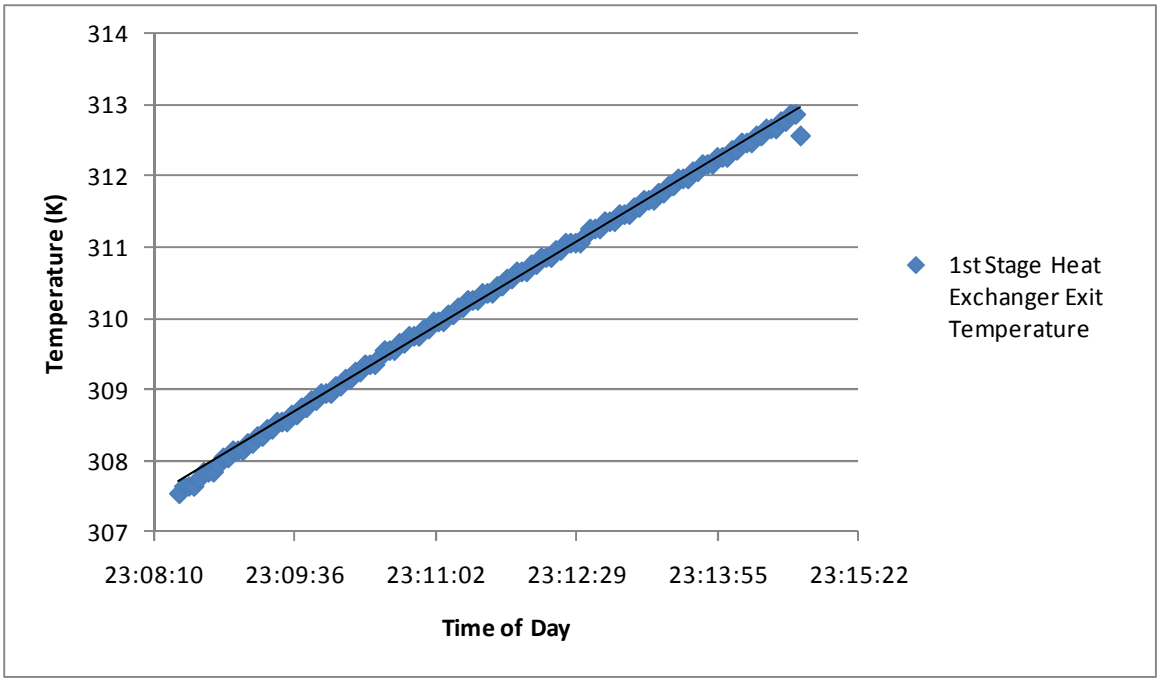

Figure 3-8 Linear regression analysis for air temperature leaving the heat exchanger.

Refer to Figure 3-8 for a plot of the 1st stage heat exchanger exit temperature. Air temperature entering the 2nd stage compressor was calculated for each time step using Eq 3.9. With these modifications CAES Simulator produced data that follow experimental trends for the air leaving the 2nd stage compressor. Figure 3-9 displays the 2nd stage exit temperature for experimental and computational results. Computational results followed the general trend of the experimental results with a less than 1% difference.

Compression within the tank was an isothermal process due to convective heat transfer to the surrounding walls of the tank. This was confirmed by calculating the experimental convective heat transfer coefficient (h) and comparing it to that of gas which typically ranges between 2-25 W/m^2 .[14] A convective heat transfer coefficient to the surrounding walls was calculated to be 1.40 $W/m^2 \cdot K$ when the tank pressure was 781.69 kPa. The convective heat transfer coefficient of the air in the storage tank

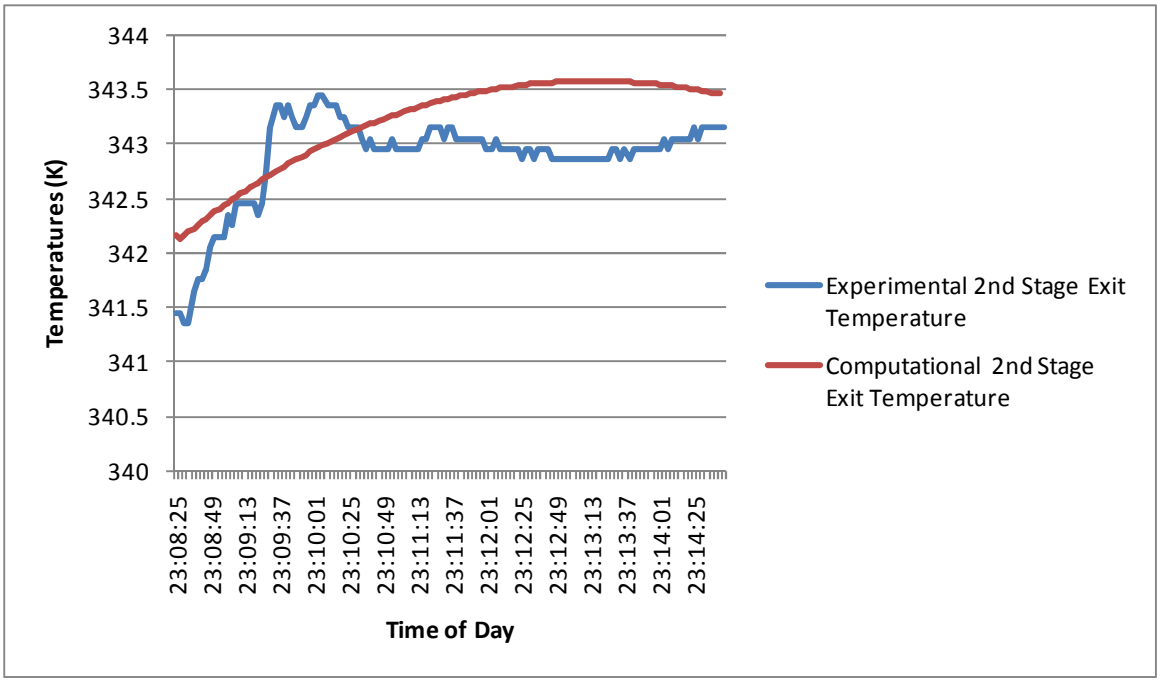

Figure 3-9 2nd stage compression exit temperature.

was calculated using the lumped capacitance method[14],

$$h = -\frac{c_{pSteel} m_{Steel}}{A\Delta t} \ln\left(\frac{T_{Final} - T_{Ambient}}{T_{Initial} - T_{Ambient}}\right) \qquad (3.13)$$

where m_{Steel} is the mass of the steel in the tank, c_{pSteel} is the constant specific heat of the steel, A is the inner surface area of the tank, Δt is the time step used in the computational model, and $T_{Initial}$ and T_{Final} are the tank wall temperatures before and after heat transfer. Refer to reference [2] for the properties of plain carbon steel. T_{Final} is the predicted temperature of the steel walls after one time step, assuming that thermal energy transfer occurred from the air to the walls of the tank. It was defined as,

$$T_{Final} = c_{pSteel} m_{Steel} (T(n+1) - T(n)) / c_{pAir} m_{Air} + T_{Initial} \quad (3.14)$$

where T(n) and T(n+1) are the computational temperature of the tank at the initial pressure and after one time step, respectively.

The Biot number (Bi) was calculated to validate the use of the lumped capacitance method. A Biot number is the ratio of resistance of convective heat transfer across the convective boundary layer to conductive heat transfer across the material and is defined as,

$$Bi = hL_c/k \quad (3.15)$$

where L_c (=Volume/Area) is the characteristic length and k is the coefficient of thermal conductivity. The use of the lumped capacitance method is validated when the ratio is low or Bi is much less than 0.1. A Bi of 2.3E-5 was calculated for the heat transfer between the air and the walls of the tank.[14]

As the tank filled, convective heat transfer to the surroundings was substantial enough to keep the tank temperature at 318 K during compression from 781.69 kPa to 1205.79 kPa. Figure 3-10 shows the temperature in the tank throughout the compression cycle. Figure 3-10 also displays the temperature in the tank when the air was released. CAES Simulator was modified to model the isothermal conditions in the tank. The isothermal conditions increased the mass storage of the tank due to the linear relation of temperature and pressure imposed by the ideal gas law. Modeling the tank as isothermal increased the charge time and decreased the efficiency of compression. The air's

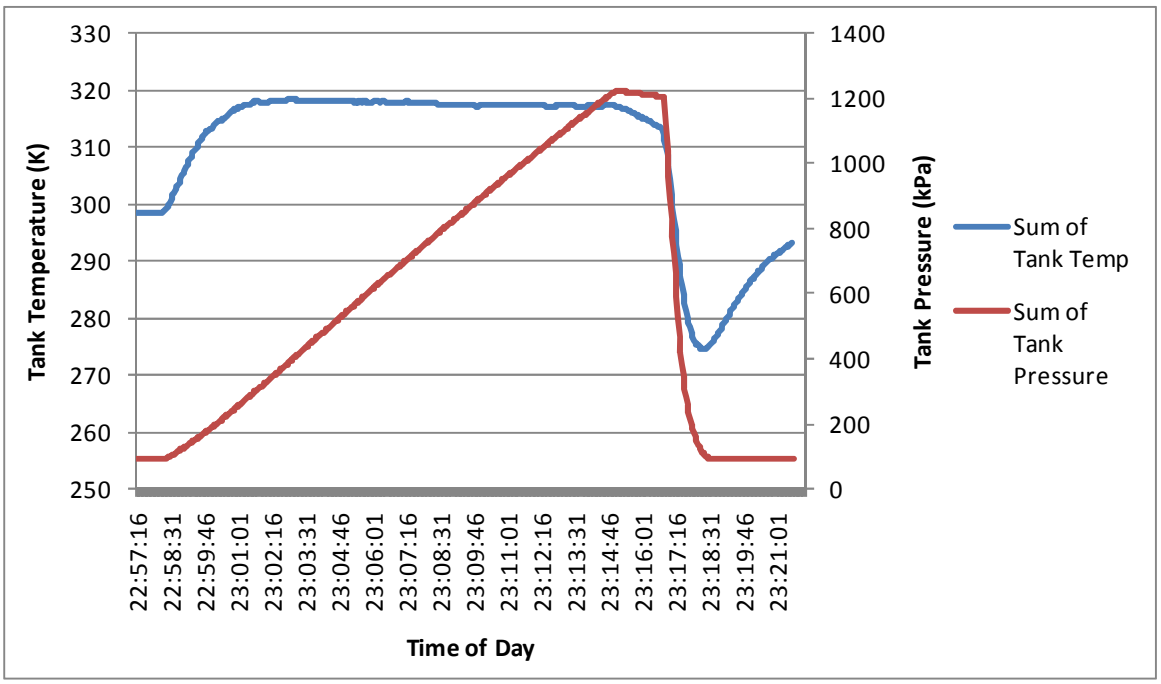

Figure 3-10 Experimental tank temperature compared to tank pressure.

decrease in density from cooling highlights the importance of a second stage heat exchanger before storage.

3.4.4 Mass Flow Data Comparison

Experimental air mass flow rates were measured using two techniques. The first method calculated the mass flow rate by applying the ideal gas law to the instantaneous pressure, temperature and humid air gas constant to find the mass of the air within the tank. As the tank filled the difference in mass at each time step was divided by the time difference,

$$\dot{m} = \frac{m(n+1) - m(n)}{\Delta t}. \qquad (3.16)$$

The second method used techniques outlined in Section 3.2.3. Equation 3.11 was also applied to the experimental data. Figure 3-11 displays the results of each method.

To test the validity of each method the mass of the air compressed into the tank was found by subtracting the final mass of 99.98 kg from the initial mass of 64.76 kg in the tank using the ideal gas law. Methods described by ASME MFC-3M-1989 produced results that agreed well with the total mass of the air compressed into the tank. The ASME method predicted a total mass transfer of 34.1 kg which differs by 3.2% from the ideal gas method.

Mass flowrates obtained by the time iterative computational model, used by CAES Simulator, also agreed well with experimental results. Compression cycles for a reciprocating piston cylinder compressor do not produce a steady flow stream of air.

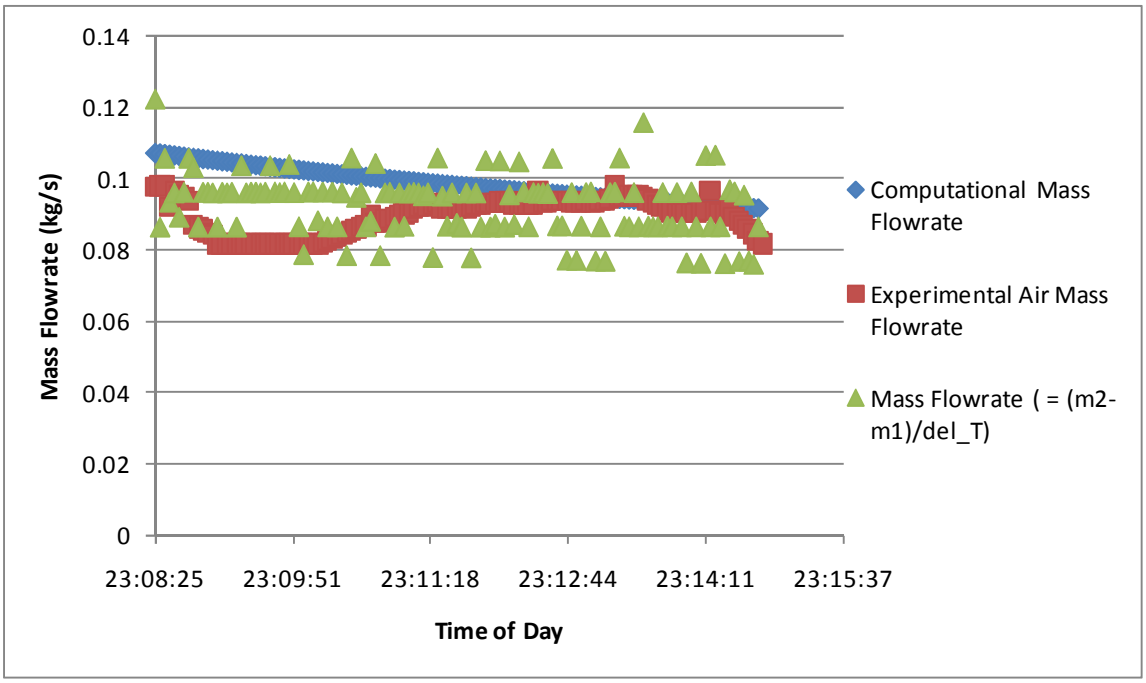

Figure 3-11 A comparison of calculated mass flow rates.

Mass flowrates oscillate as the compressor's piston travels between a suction and compression stroke. The oscillation of the compressor's piston accounts for the difference between the computational and experimental mass flowrates which differ by less than 3% at any point in time. CAES Simulator is also not equipped to predict heat losses from the air storage vessel but does approximate the thermodynamic properties of the air during isothermal compression within a high degree of accuracy, once the tank temperature trends have been established.

3.4.5 Energy Comparison

CAES Simulator's computational model is controlled by the mechanical and adiabatic efficiency of the compressor, turbines and heat exchangers. The system efficiency is governed by the ability of each piece of equipment to effectively use the municipal electrical power input to the system. CAES Simulator determines the amount of irreversible thermal energy losses from the system using user defined mechanical efficiency and the polytropic coefficient. From these two variables the computational model can determine how much energy is transferred to the shaft of the compressor and turbine and how much energy is lost as heat.

The main benefit of an AA-CAES plant is its ability to store and reuse thermal energy. During the heat exchange process the air transfers energy through sensible and latent heating. Using Eq. 3.3, the thermal energy transferred to the 1st stage heat exchanger was calculated and plotted in Figure 3-12. It should be noted that CAES Simulator predicted condensation during the 1st stage heat exchanger cycle but that the effects of latent cooling were minimal. Figure 3-12 also displays the computational 1st

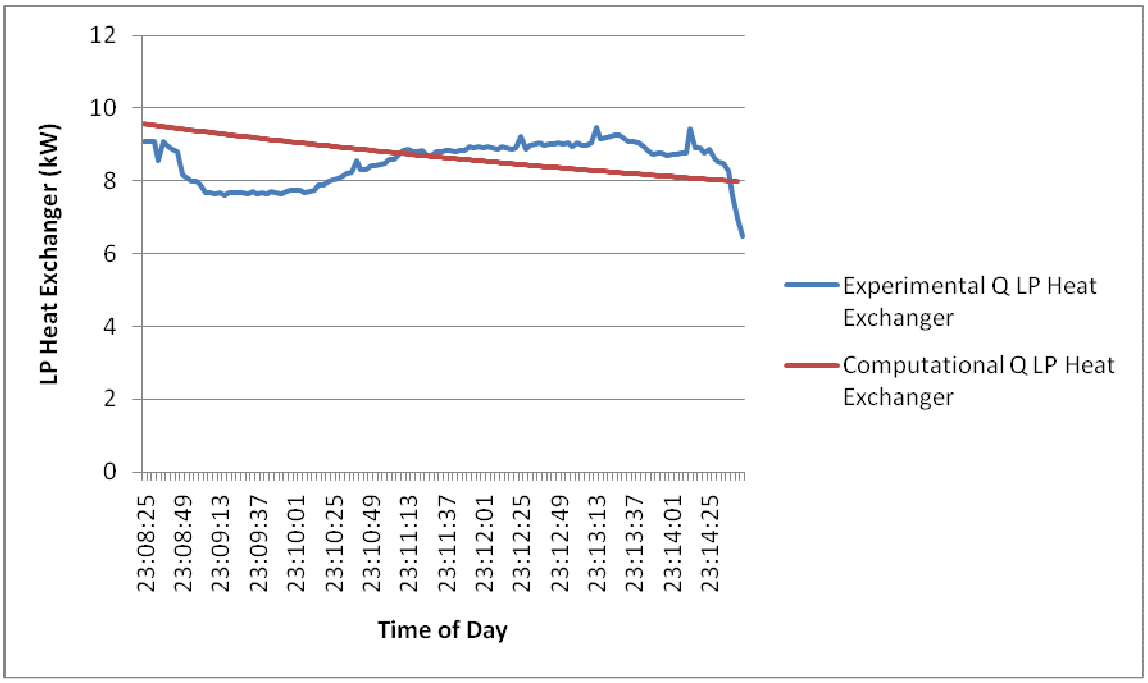

Figure 3-12 1st stage heat exchanger thermal energy transfer.

stage heat exchanger results produced by the CAES simulation. Computational results at each time step differed from experimental results by as much as 22.1% but averaged 7.4% overall. Nonsteady mass flowrates account for the unsteady behavior of the experimental heat transfer results. The methods used to determine heat transfer in the 2nd stage heat exchanger were identical to methods used for the 1st stage heat exchanger. For this reason a comparison study for the 2nd stage heat exchanger was not conducted.

3.5 Conclusion

This comparison study demonstrated CAES Simulator's use of a computational time iterative thermodynamic model to produce results that matched experimental data of a two stage compressor. The comparison study demonstrated the ability of CAES

Simulator to calculate temporal changes of pressure, temperature and humidity as the air cycled through the compression and heat exchange cycles. The computational model required manipulation to precisely model experimental conditions such as heat transfer to the surroundings.

Polytropic efficiencies were sensitive to heat transfer during compression. The assumption that the polytropic efficiency remained constant throughout the experiment proved to be invalid. Between the selected pressures, γ increased by 0.8 % during the 1st stage compression and decreased by 2.1% during 2nd stage compression. Although these changes were small, as exponents of the polytropic relations between pressure and temperature, the polytropic coefficients have a large effect on temperature and pressure calculations.

Discrepancies between the computational and experimental results were a product of the model's use of constant input conditions such as γ and the 2nd stage compressor's inlet temperatures. As the pressure ratio in the 2nd stage compression cycle increased the compressed air temperature leaving the 2nd stage compressor increased. Inlet water to the 1st stage heat exchanger is first heated by thermal energy transferred during the 2nd stage heat exchanger. The approach between the inlet water and the compressed air in the 1st stage heat exchanger decreased as the inlet water temperature increased. The thermal capacity of the 1st stage heat exchanger was reduced as the inlet approach decreased. Additionally, the system lost heat to the walls of the storage tank.

CAES Simulator does not have the ability to predict heat loss to the environment without obtaining experimental trends and manipulating the model to account for experimental conditions. Users of CAES Simulator must take care to either eliminate

heat losses, made apparent by this comparison study, or modify the computational model to match changing boundary conditions. Equipment selection will be a critical component to eliminating energy losses and ensuring the overall plant efficiency. Despite complications with predicting thermal losses to the environment, CAES Simulator was able to predict mass flowrates to within 3% accuracy and heat exchanger thermal energy transfer to within 7.4% on average.

CHAPTER 4

RESULTS AND DISCUSSION: COTTONWOOD CANYON MINE FEASIBILITY STUDY

4.1 Introduction

The performance of a compressed air energy storage plant is highly dependent on the location of the facility, weather conditions at the site, and equipment limitations. CAES Simulator is controlled by the user defined conditions, such as ambient air properties and equipment specifications, which CAES Simulator uses to produce time series data that models the conditions of potential CAES systems. To accurately model the overall efficiency of an AA-CAES system, hourly weather data must be collected to define thermodynamic properties of the working fluid air. The following section examines the conditions at a potential site in the mine shafts of Cottonwood Canyon, Utah. Data pertaining to ambient weather conditions will be used to model an AA-CAES plant using CAES Simulator and the computational results will be analyzed to determine the feasibility of installing a plant at the Michigan-Utah Mine location.

4.2 Michigan-Utah Mine

4.2.1 Mine Characteristics

This study will examine the use of Michigan – Utah mine as a storage vessel for an advanced adiabatic compressed air energy storage plant. Located between the ski resorts of Alta and Solitude at N 40.600506 and W-111.611589, the Michigan – Utah mine is a conglomerate of vertical shafts and massive stopes. The entrance of the mine starts at a horizontal shaft called Cleve Tunnel. Cleve Tunnel is joined with stopes at approximately 1500 ft into the base of the mountain at an elevation of 9316 ft above sea level. The honeycomb cliffs are directly above the Cleve tunnel with the highest point of the mountain at an elevation of 10,472 ft above sea level. Walls of the mine are comprised mostly of limestone rock. Michigan – Utah's size, location and structure make it an ideal candidate for an AA-CAES plant.

The AA-CAES electrical capacity is limited by the size of the storage vessel and its ability to contain pressurized air. Additional vertical shafts connect the Cleve tunnel to the Topeka tunnel and a network of shafts called City Rocks. The modularity of this mine is ideal for sizing an AA-CAES plant. Output of the plant can be controlled by sealing sections of the mine and opening them as further storage is needed. The Cleve Tunnel mine and its adjoining stopes sits beneath 1156 ft of limestone rock. A further geological study of the site must be performed before it is determined if the shafts are suitable as cyclic pressure vessels though it is generally accepted among geologists that the hydraulic gauge pressure is 22.6 kPa per meter of overburden.[15] A water curtain above the shafts would further aid in sealing the pressurized air storage.

4.2.2 Weather Data

The high mountainous terrain of Alta, Utah experiences a variety of weather conditions throughout the year. During the summer months, (May through September), Alta is a warm humid climate collecting moisture from snow melt. During the winter months, October through April, temperatures are typically below freezing. Humidity levels drop during the winter months due to the low temperatures and high altitude. Alta has averaged 202.4 cm of snowfall per month over the last 29 seasons.[16]

Weather data for the Michigan – Utah mine were collected using the University of Utah's MesoWest weather data base. Temperature and relative humidity data were recorded from a meteorological station positioned on the top of Collins Mountain at Alta Ski Resort. Alta's weather tower is located at a height of 10,443 ft above sea level and approximately 2 miles away from the entrance of Cleve Tunnel. Data were collected for one year starting on December 16, 2008. Temperatures ranged between -23.15 and 22.79˚C. Relative humidity ranged between 3 and 97%. Refer to Figures 4.1 and 4.2 for hourly temperatures and absolute humidity levels for the year.

Temperature and absolute humidity data were tabulated on a frequency plot to map hourly conditions. Peak electrical use hours are between 13:00 and 19:00. For the purpose of this study, it was assumed that the compressor would run for 8 hrs before the expansion cycle. Data between the hours of 04:00 and 12:00, which were assumed to be the compressor operating hours, were separated from the remaining data. Temperatures were grouped in ranges of 1˚C starting at -22˚C and ending at 20˚C. The column entitled "Number of Hours Between 4:00 and 12:00 displays the number of hourly readings that fell within the 1˚C range. This method was repeated for absolute humidity data using

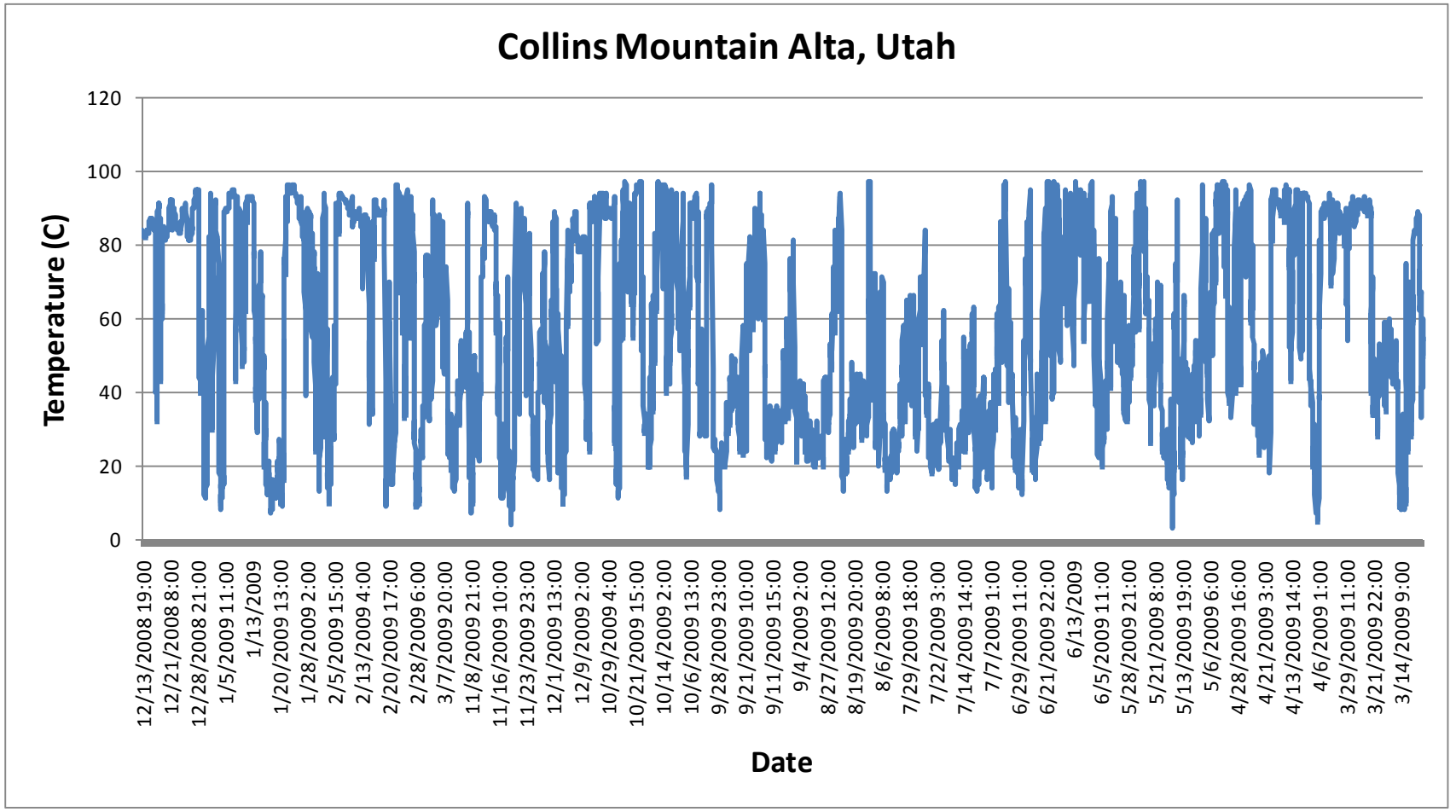

Figure 4-1 MesoWest hourly temperature data for Collins Mountain Alta, Utah.

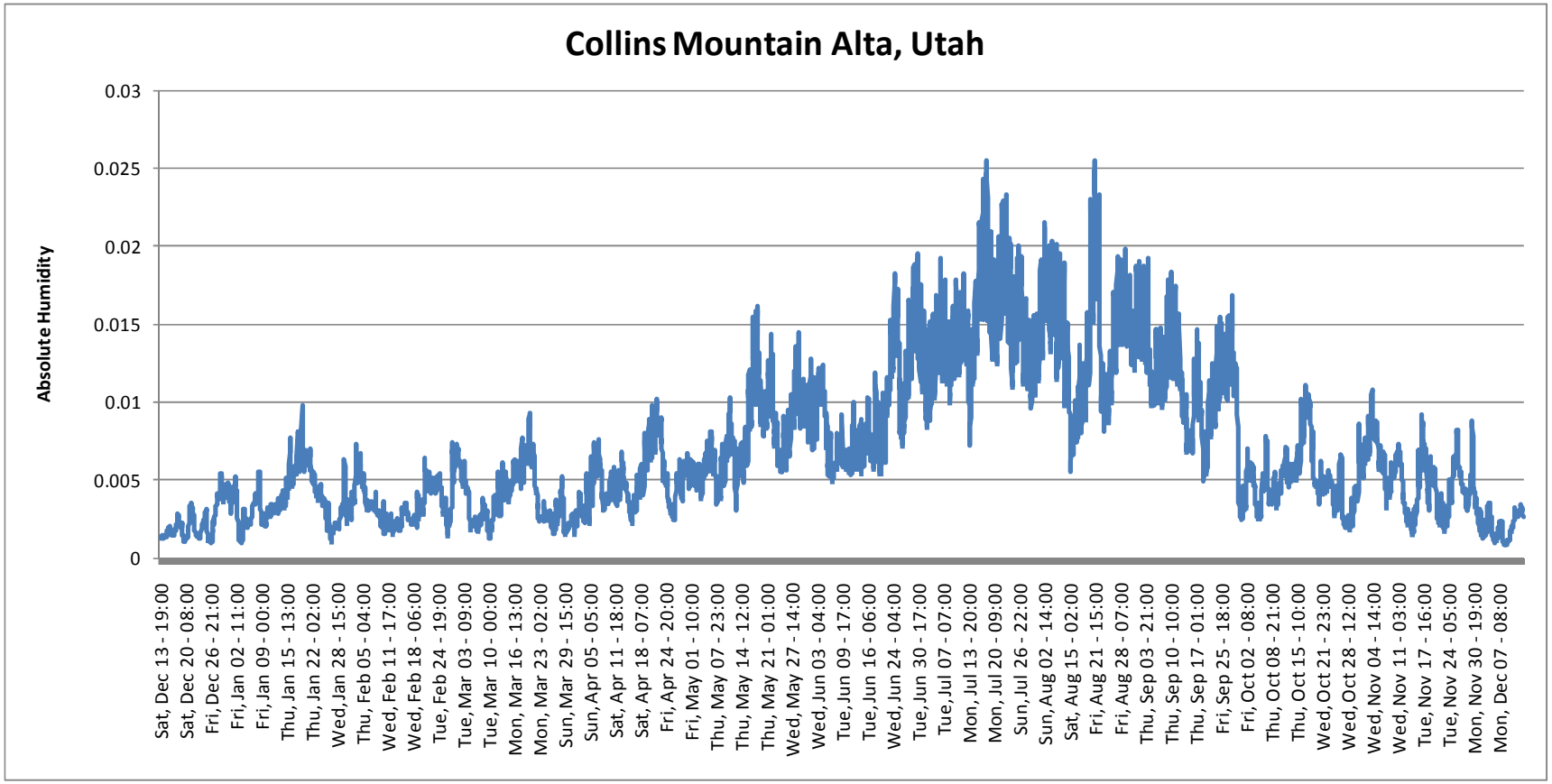

Figure 4-2 MesoWest hourly absolute humidity data for Collins Mountain Alta, Utah.

increments of 0.001g H_2O/ g dry air. Absolute humidity was derived from the MesoWest weather data using techniques described in Section 3.2.1. Atmospheric pressure was assumed to be 70.55 kPa. Figure 4-3 displays tabulated frequency weather data for the site. Weather frequency plots were used to map the environmental conditions of the outdoor air. As shown in Figure 4-3(a), temperatures were below freezing 50% of the time during the hours between 04:00 and 12:00 throughout the year. Air moisture content levels were below 0.001g H_2O/ g dry air, 77.8% of the time during these hours.

4.3 Michigan-Utah Mine AA-CAES Simulation Results

4.3.1 Introduction

To demonstrate the ability of an AA-CAES to function in Cottonwood Canyon, CAES Simulator was configured with a variety of potential ambient conditions, equipment limitations and other boundary conditions associated with a prospective plant design. The effects of changing ambient conditions such as temperature and humidity were studied to identify how they affect the efficiency of a plant. The following sections outlines techniques used to analyze ambient air inlet conditions and their effects on the performance of an AA-CAES.

4.3.2 Cottonwood Canyon Mine AA-CAES Computational Setup

CAES Simulator was configured to model a 100 MW plant using 1,000,000 m^3 of

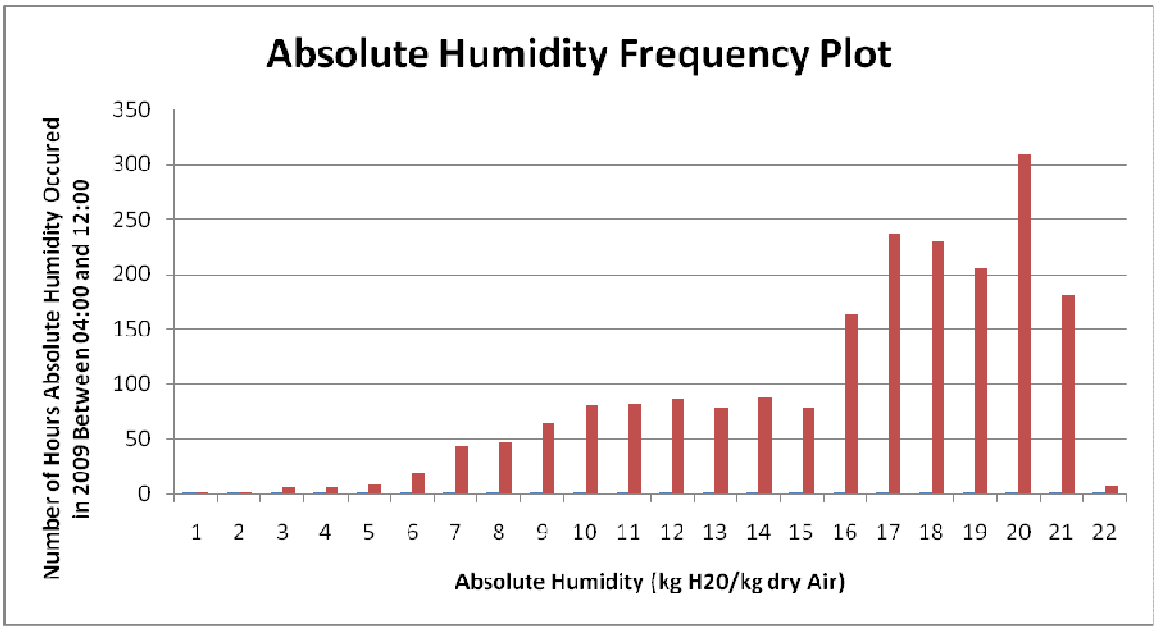

(a)

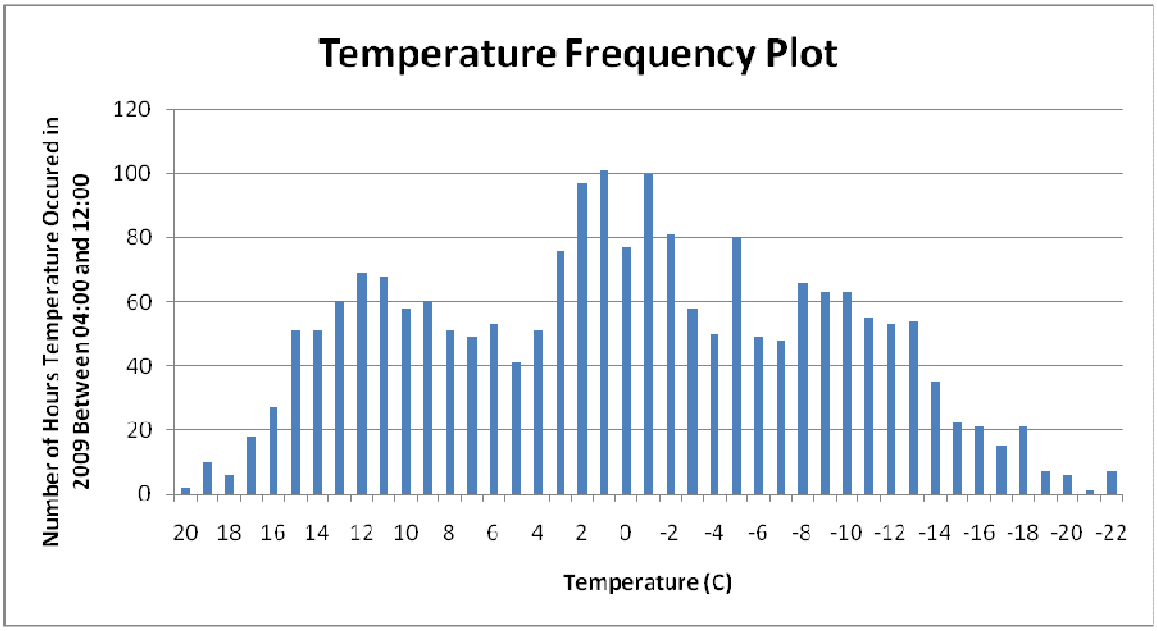

(b)

Figure 4-3 Frequency plot of the temperature (a) and absolute humidity (b) weather data for Collins Mountain Alta Utah.

underground storage. Production size and storage were selected as multiples of 10 so that they could be scaled with ease. A production of 100 MW was chosen because the scale is similar to the two existing plants in Huntorff, Germany and Alabama, US. A geological survey of the mines must be performed before accurate storage dimensions can be modeled but 1,000,000 m^3 is a reasonable approximation of the space within the mine. Tank pressures were modeled to cycle between 4137 and 7585 kPa. Maximum tank pressure was determined by assuming an over burden of 335 m with a gauge pressure gradient of 22.6 kPa per meter of over burden. Turbo machinery used in an AA-CAES facility must operate at high efficiencies and handle extreme temperatures to ensure minimal mechanical and thermal energy losses. The turbine and compressor efficiencies were assumed to be constants of 0.9 and 0.85, respectively. Adiabatic efficiencies for the compressor and turbine were assumed to be constant at 0.97. During the computational simulations, the compressed air reached exit temperatures in excess of 567˚C. Turbine entrance temperatures were modeled as high as 417˚C.

Plant configurations were determined by defining temperature and pressure set points at eight specific positions within the AA-CAES cycle. These set points include the HP and LP turbine inlet temperature, the HP and LP turbine exit pressure, the HP and LP compressor inlet temperature, the LP compressor exit pressure and the tank inlet temperature. By adjusting each of these set points and using turbine and compressor efficiencies of 0.9 and 0.85, an optimal overall plant efficiency of 74.9% is obtainable using the machinery efficiencies previously defined. To reiterate this point, the AA-CAES incurs losses due to the mechanical and thermal inefficiencies of the machinery and for this reason cannot achieve efficiency greater than 75%.

Temperature, pressure and humidity are measured properties that govern other thermodynamic properties of air such as specific heats and gas constants. Simulations were run with various ambient air properties, typical of the range of gathered weather data, to demonstrate how ambient conditions affect the efficiency of the proposed Michigan – Utah mine AA-CAES facility. Plant configurations were adjusted to achieve an efficiency of 75% at the minimum value of the temperature, pressure and absolute humidity ranges that were found in the collected weather data at Collins Mountain, Alta.

4.3.3 Ambient Air Temperature Effects on an AA-CAES

Temperature ranges of ambient air entering an AA-CAES affect the thermodynamic limits of equipment by changing the operating temperature and pressure ranges required to achieve optimal plant efficiency. As ambient temperatures rise the heat exchangers must extract larger amounts of thermal energy from the incoming air. Turbine inlet temperatures must also rise to affectively transfer the increase in thermal energy that was extracted during compression, to the discharged air. Compressor discharge air temperatures increase with an increase in ambient air temperature. The effects of changing ambient temperatures can be seen in Figure 4-4.

CAES Simulator was used to model an AA-CAES plant at the Michigan-Utah Mine with varying ambient air temperature and humidity conditions. A minimum ambient air temperature and absolute humidity of -22˚C and 0.001 g H_2O/g dry air, respectively, were recorded at the weather station near the Michigan-Utah Mine during 2009. For this reason the plant was configured for an efficiency of 75% when ambient air temperatures were at a minimum of -22˚C and absolute humidity levels were 0.001 g H_2O/ g dry air.

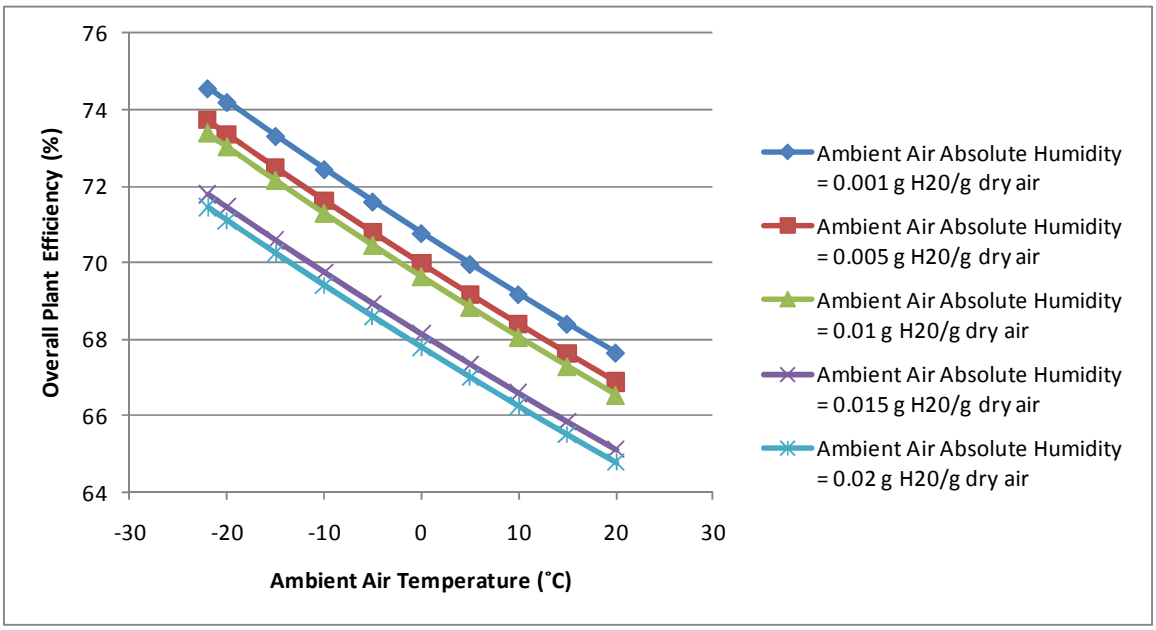

Figure 4-4 Temperature effects on the overall efficiency of the Michigan-Utah Mine AA-CAES simulation.

Plant equipment limits were incrementally adjusted until computational results achieved an overall plant efficiency of 75% using the minimum recorded ambient air temperature and humidity conditions at the weather station near the Michigan-Utah mine. Pressures between the compression and turbine cycle were determined by incrementally changing the pressures, within the computational model, until minimum compression and maximum turbine work energy were computed. HP turbine and LP compressor exit pressures were set to 760.55kPa and 1449.55kPa, respectively. HP and LP turbine inlet temperatures were incrementally increased to 417˚C. The amount of thermal energy required to elevate the turbine inlet temperatures to 417˚C was equal to the thermal energy extracted during the compression cycle.

The LP turbine exit temperature limits the minimum temperature the TES can achieve. Air storage inlet temperature is dependent on the LP turbine exit temperature. As air pressure entering the HP turbine is reduced, due to the release of air in the air storage, the turbine exit temperature decreases. Before the air passes through the LP expansion cycle, the air cools the TES during the heat exchange process. The first law of thermodynamics governs that air exiting the turbine cannot cool the TES below the minimum exit temperature of the turbine. Air discharged from the HP compression cycle is first cooled by the TES before it is stored in the air storage. The amount of air the air storage can contain is increased by decreasing the air inlet temperature. For this reason, air inlet temperature was set to the minimum TES temperature, which correlates to the minimum HP turbine discharge temperature. An air storage inlet air temperature of 318˚C was set for the computational model. Using the plant configuration outline in this and the previous paragraph, simulations were run for ambient air temperatures in the range of -22 to 20˚C. Simulations were repeated for absolute humidities in the range of 0.001 to 0.02 g H_2O/ g dry air in 0.005 increments. Figure 4-4 displays a plot of the effects ambient humidity and temperature have on the overall efficiency of the proposed Michigan-Utah AA-CAES plant.

As shown in Figure 4-3, inlet air temperature increased, the overall plant efficiency declined. The user defined inlet HP compressor and tank temperature set points govern the amount of compression stage thermal energy exchange required to cool the air. The expansion cycle heat exchanger's thermal energy transfer is defined by the turbine inlet air temperatures, which are also predefined and constant. Thermal energy extracted during compression increased without increasing the thermal energy transferred

to the air during the expansion cycle. Refer to Figure 4-4 for a graphical display of the effects of temperature and humidity on the amount of thermal energy recovered for the Michigan-Utah Mine simulation. A decline in efficiency is due to the amount of thermal energy stored in the heat exchanger that is not used to heat the air during expansion. Overall efficiency for the Michigan-Utah Mine simulation declined 9.2% as ambient air temperature was increased over the 42˚C range holding absolute humidity constant at 0.001 g H_2O/ g dry air. The unrecovered energy, or difference between the thermal energy collected during the compression cycle and the thermal energy recuperated during the expansion cycle, increased by 305.9 kJ as ambient air temperature was increased as the ambient temperature increased by 42˚C holding absolute humidity constant at 0.001 g H_2O/ g dry air.

A rise in temperature also increases the required compressor work during 1st stage compression. Figure 4-5 displays the effect of varying temperatures on the compression cycle of the Michigan-Utah AA-CAES simulation. An increase in ambient air increases the 1st stage compressor work linearly. Refer to Equation 2-23. Figure 4-6 displays the effect of varying temperatures on the work performed during the compression cycle of the Michigan-Utah AA-CAES simulation. The work required for 2nd stage compression is independent of ambient temperatures because the 1st stage heat exchanger returns the inlet temperature to a constant user defined set point. Compressor work for the Michigan-Utah Mine simulation increased 208.1 GJ increased over the 42˚C range holding absolute humidity constant at 0.001 g H_2O/ g dry air.

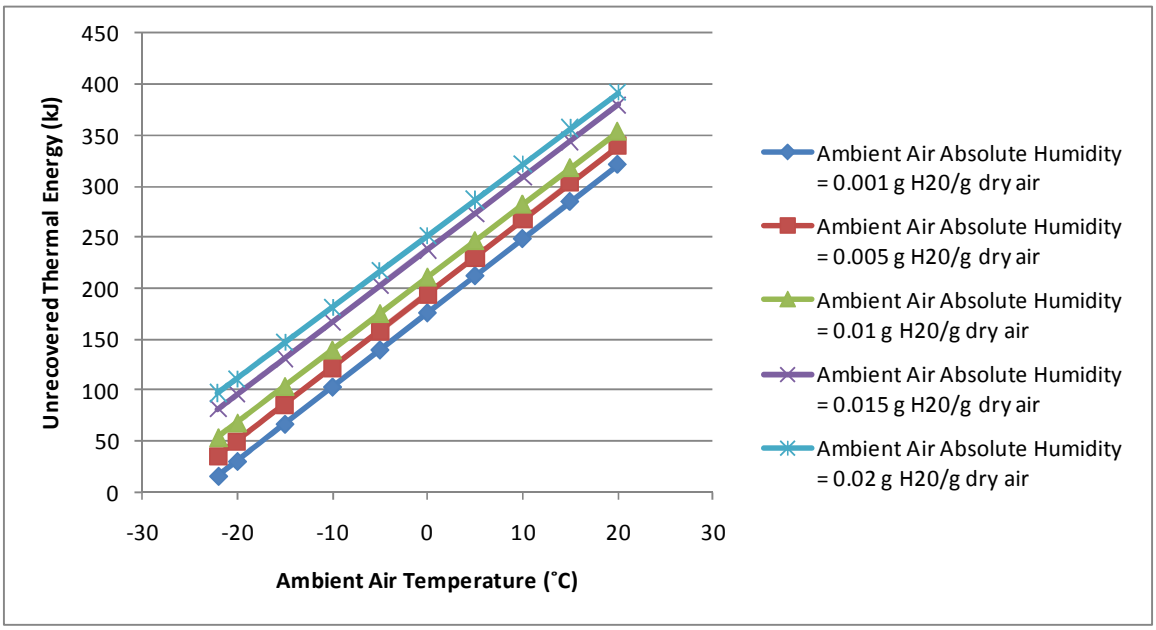

Figure 4-5 Temperature and humidity effects on unrecovered thermal energy during expansion for the Michigan-Utah Mine AA-CAES simulation.

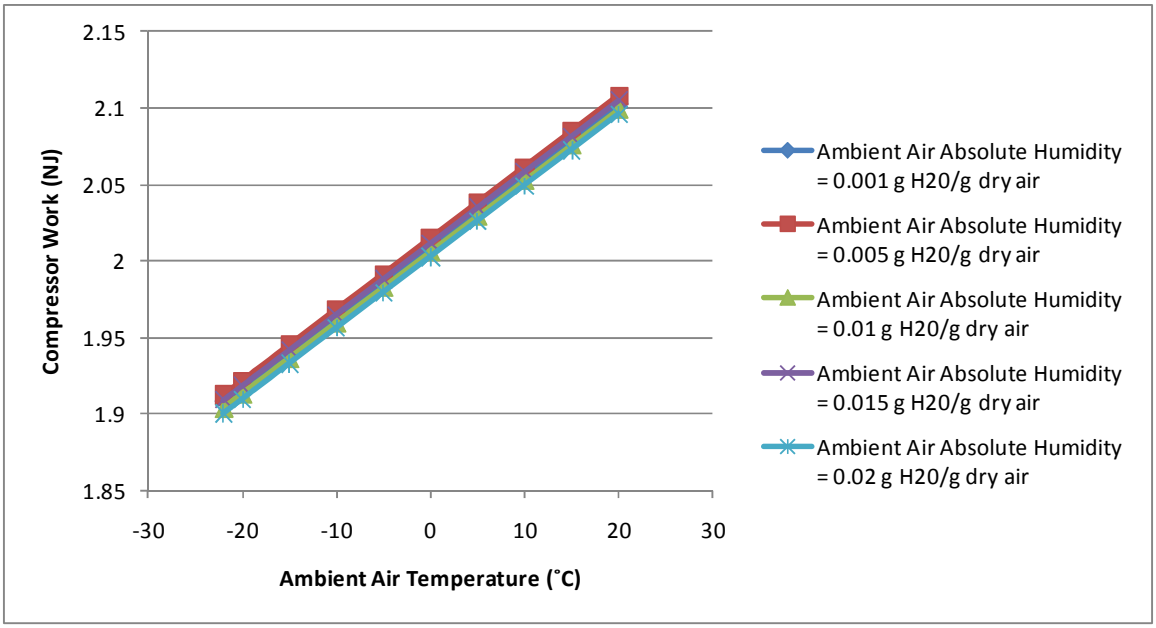

Figure 4-6 Temperature effects on the compressor work of the Michigan-Utah Mine AA-CAES simulation.

4.3.4 Ambient Air Absolute Humidity Effects on an AA-CAES

Humidity levels affect the overall efficiency of an AA-CAES cycle by altering the thermodynamic characteristics of the working fluid. Refer to Figure 4-4 for a graphical display of the affects of absolute humidity on an AA-CAES plant. Increases in ambient air humidity reduced the overall efficiency of the Michigan- Utah Mine simulation. The specific heat capacity of air increases with the addition of water vapor. During compression the temperature of the exiting air increased with a rise in humidity. The simulation's overall efficiency of the plant was reduced due to the expansion cycle heat exchanger's inability to transfer all of the thermal energy extracted during compression. Overall efficiency for the Michigan-Utah Mine simulation declined 3.23% with a 0.019 g H_2O/ g dry air change for an ambient temperature of 22˚C. The amount of heat not recovered increased by 53 GJ with a humidity increase of 0.019 g H_2O/ g dry air.

Humidity levels also had an effect on compressor and turbine run times. Refer to Table 4-1 for the effects of humidity on the Michigan-Utah Mine simulation. During the Michigan-Utah Mine simulation the compressor and turbine run times were 7320 and 6420 seconds, respectively, when absolute humidity was set to 0.001 g H_2O/ g dry air. Run times increased as the absolute humidity levels were incrementally raised. Compressor and turbine run times were 7440 and 6720 seconds, respectively, for an absolute humidity of 0.02 g H_2O/ g dry air. The final tank temperature for the simulation using 0.02 g H_2O/ g dry air humid ambient air exceeded the 0.001 g H_2O/ g dry air by 3.54˚C. Turbine run times decreased due to the reduction in heat recovery. The amount of heat recovery decreased due to the limitations placed on the expansion heat exchangers

by the turbine inlet temperature set points. Refer to Table 4-1 for a tabulated list of values.

4.3.5 Ambient Air Pressure Effects on an AA-CAES

Ambient pressure levels affect the operation of an AA-CAES by changing the amount of potential energy the tank can store. Pressure differences between the ambient air and the storage tank drive the amount of work that can be produced by the turbine. Simulations were run for ambient air pressures between the range of 66 to 74 kPa, in 2 kPa increments, using the plant configuration outlined in Section 4.3.3. When using the plant configuration described in Section 4.3.3, a reduction in pressure resulted in a reduction in compressor and turbine work. For this reason the AA-CAES model was configured for a 75% efficiency at an ambient pressure of 74 kPa, which is at the upper limit of the range of ambient pressures simulated

Changing ambient pressures effect the exergy of the proposed Michigan-Utah plant. Exergy is the total energy of a system, subtracting the irreversible energy, leaving

Table 4-1 Effects of ambient air humidity levels on the Michigan-Utah Mine simulation.

Absolute Humidity (g H2O / g dry Air)	Compressor Run Time (sec)	Turbine Run Time (sec)	Compressor Work (GJ)	Turbine Work (GJ)	Overall Plant Efficiency (%)	Heat Exchanger Input (GJ)	Heat Exchanger Output (GJ)
0.02	7440	6720	1908	6720	74.6	1715	1670
0.015	7440	6660	1912	6660	73.7	1719	1683
0.1	7380	6600	1904	6600	73.4	1719	1666
0.005	7380	6480	1909	6480	71.8	1723	1641
0.001	7320	6420	1900	6420	71.4	1723	1626
Ambient Temperature= -22˚C, Ambient pressure =70.55 kPa							

only the useful quantity of energy. For an AA-CAES, exergy is the potential for the compressed air, held within the air storage, to perform work on the turbines. Exergy of a compressed air tank is defined as,

$$X = m\left[\left(u_1 - u_0\right) + P_0\left(\frac{1}{\rho_1} - \frac{1}{\rho_0}\right) - T_0\left(s_1 - s_0\right) + \frac{V_1^2}{2} + gz_1\right] \qquad (4\text{-}1)$$

where m is the mass in the tank and the subscript 1 and 0 refer to the conditions in the tank and ambient conditions, respectively. Assuming the effects of gravity and kinetic energy are negligible and that the internal energy entering the tank is equal to the internal energy of the ambient air, Equation 4-1 reduces to,

$$X = m\left[P_0\left(\frac{1}{\rho_1} - \frac{1}{\rho_0}\right) - T_0\left(s_1 - s_0\right)\right]. \qquad (4\text{-}2)$$

Assuming the air behaves like an ideal gas Equation 4-1 can be rewritten as,

$$X_1 = mRT_0\left(\ln\frac{P_1}{P_0} + \frac{P_0}{P_1} - 1\right). \qquad (4\text{-}3)$$

Refer to Reference 9 for a detailed derivation of the Equation 4-3.

The available exergy decreased with the rise of ambient pressure. Refer to Table 4-2 for the effects of changing ambient air pressure on the Michigan-Utah Mine. Tank pressure limits restrict the amount of exergy available from the pressure difference between the tank and ambient air. Although the work required to pressurize the air

Table 4-2 Effects of ambient air pressure levels on the Michigan-Utah Mine simulation.

Ambient Air Pressure (kPa)	Compressor Run Time (sec)	Turbine Run Time (sec)	Compressor Work (GJ)	System Exergy (GJ)	Overall Plant Efficiency (%)	Heat Exchanger Input (GJ)	Heat Exchanger Output (GJ)
66	7440	6720	1945	1435	73.75	1753	1691
68	7440	6720	1929	1430	74.14	1736	1692
70	7440	6660	1912	1411	74.80	1719	1676
72	7440	6660	1897	1407	74.16	1704	1677
74	7440	6660	1882	1402	74.50	1689	1678
Ambient Temperature= -22˚C, Ambient Absolute Humidity =0.001 g H2O/ g dry Air							

decreased with the pressure difference, the ability of the turbine to produce work was also reduced. Work required for compression decreased by 63 GJ over the 10 kPa increase in ambient pressure. Work produced by the turbine decreased by 60 GJ. The efficiency of the compressor is less than the efficiency of the turbine which accounts for the discrepancy between compression and expansion energy loss. The overall efficiency was reduced less than 1% for an ambient air 10 kPa reduction. These changing ambient air pressures are of little consequence when compared to the losses incurred by ambient temperature changes.

4.4 Michigan-Utah Mine AA-CAES Design Discussion

The Michigan-Utah Mine AA-CAES plant's overall efficiency is limited by the efficiency of its machinery. Changes in temperature, pressure and absolute humidity affect the operation of an AA-CAES system. Utah's cold dry climate is ideal for an advanced compressed air energy storage plant. Michigan-Utah Mine experiences temperatures below freezing over 50% of the year. Colder temperatures allow for lower design temperatures when considering turbines, compressors and the size of thermal

energy storage. Cottonwood Canyon's low humidity levels will also aid in reducing the operational temperatures of the plant.

Declining efficiency caused by an increase in ambient temperature and absolute humidity can be reversed by increasing the heat transfer and temperature of the air entering the turbine. The collected weather data showed small changes in temperature during the compression operational hours. The collected weather data displayed an average of 4˚C rise in temperature, between the hours of 04:00 and 12:00, throughout the year. An increase in ambient temperature requires additional work from the compression cycle. A rise in compression work translates into higher temperatures at the exit of the compressor. Compression cycle heat exchangers must extract larger quantities of thermal energy to maintain 2nd stage compressor and tank inlet temperatures as ambient temperatures rise.

Increasing turbine inlet temperature allows more thermal energy recovery during the expansion cycle heat exchange process. HP and LP turbine inlet temperature, HP and LP compression heat exchanger discharge temperature, LP compressor exit pressure and the tank inlet temperature control the operation of an AA-CAES plant. These six control points must be fine tuned and monitored during the plant's operation to maximumize efficiency.

The Michigan-Utah Mine must contain efficient equipment capable of handling high pressures and temperatures. Compressors must be designed for pressures and temperatures that have a minimal range of 0 to 7585 kPa and -22 to 588˚C, respectively. Turbines must be designed for pressures and temperatures that have a minimal range of 0 to 7585 kPa and -22 to 588˚C, respectively. Machinery must be insulated to prevent

thermal losses to the environment. A thermal energy storage vessel must be selected capable of containing thermal energy loads in excess of 2278.29 GJ and reach temperatures exceeding 588˚C. A geological survey must also be completed to identify the structural integrity and size of the compressed air storage vessel. If these specifications can be met the Michigan-Utah Mine simulation indicates that this is a suitable location for an AA-CAES location.

CHAPTER 5

CONCLUSIONS AND FUTURE WORK

5.1 Conclusions

This study examined the feasibility of the operation of an advanced adiabatic compressed air energy storage plant at the Michigan-Utah Mine located in Cottonwood Canyon, Utah. The development of the computational model software package, CAES Simulator, made it possible to model the effects of changing ambient air conditions and varying plant configurations to achieve maximum overall efficiency. Recommendations for the design of the proposed facility are based on the results of the simulation. The following conclusions are made from the results of this study:

1. A number of environmental conditions affect the adiabatic efficiency of a compressor and turbine. A real world compressor cannot be perfectly insulated and experiences unsteady heat transfer losses to its surroundings. To accurately model the exact solution of an AA-CAES simulation, compressor data relating to the performance of a compressor must be collected during its operation. Adiabatic efficiencies are not constant and should be modeled according to trended data.
2. Adiabatic efficiency has a large impact on the effectiveness of a compression cycle. Losses occurring during compression reduce the amount of thermal energy that can be

recovered during expansion. Compressor trains that require limited cooling lubrication and that can be insulated are ideal candidates for an AA-CAES plant. The Michigan-Utah Mine simulation used an adiabatic efficiency of 97% while still achieving an overall efficiency of 75%.

3. The overall efficiency of an AA-CAES is limited by equipment limitations and thermal energy losses. Machinery must be designed to withstand temperatures ranging from below freezing to an excess of 650˚C while maintaining operation with high efficiency. The feasibility of an AA-CAES will be determined by the availability of equipment meeting these requirements.
4. Ambient temperatures affect amount of thermal energy storage required. An increase in ambient air temperature requires additional thermal energy recovery during the expansion cycle heat exchange. Turbine inlet temperatures must be increased to account for the additional load.
5. Humidity levels affect other intensive properties of the air. A rise in humidity increases the specific heat capacity of air. Humid air experiences a greater rise in temperature during compression than dry air. This rise in temperature requires larger heat recovery and increases the operating temperatures of the AA-CAES cycle.
6. Ambient pressure has little effect on the overall efficiency of an AA-CAES plant. Operational pressures are limited by the ability of the storage vessel to contain pressurized air. Tank pressures should always be pressurized to their upper limits. Changes in pressure affect the available exergy between the ambient air and pressure within the storage vessel. The capacity of compressed air storage is affected by changes in ambient pressure.

7. The volume of pressurized air and thermal energy storage limits the capacity of an AA-CAES plant. A larger volume of storage allows the facility to produce larger amounts of work. This translates into higher wattages or longer run times.

5.2 Future Work

The next phase of this study is to design a thermal energy storage system capable of storing the thermal loads produced by an AA-CAES. Thermal energy storage is the keystone to the success of a completely emissions free CAES facility. A thermal storage device (TES) would have to minimize losses to its surroundings, effectively transfer all of the recovered energy, and discharge thermal energy at a controlled rate. As demonstrated by this study, an AA-CAES's overall efficiency is the product of its equipment. CAES Simulator could be programmed to model actual heat exchange between the TES and pressurized air. CAES Simulator would include the effects of losses such as fouling and conductive heat transfer to the surrounding walls. CAES Simulator would be programmed to show how varying heat transfer rates affect the performance of the plant. Accuracy could also be improved by adding the capability of subroutines that simulate real world adiabatic efficiencies.

Environmental effects, of heat losses from equipment, can have an effect on the adiabatic efficiency of the machinery used in an AA-CAES plant. CAES Simulator could be equipped with the ability to take experimental data and modify the computational model to implement algorithms, based off experimental trends, to identify necessary improvements in the plant design. The implementation of algorithms based off experimental data would aid in equipment selection and plant configuration.

CAES Simulator's main function is to model varying plant configurations to optimize the overall efficiency for the various environmental conditions of a potential site. CAES Simulator would be greatly improved if it could produce efficiency maps for ambient weather conditions. The user would input equipment limitations and weather data and CAES Simulator would produce the effects of changing ambient conditions on the potential AA-CAES system. CAES Simulator could also be programmed to identify the six control points which would optimize the system.

CAES Simulator proved to be an effective and accurate tool for predicting the operation of an AA-CAES system. The addition of the previously mentioned modifications to the simulation software would allow it to model an AA-CAES facility with a higher degree of accuracy.

APPENDIX A

COMPUTATIONAL CODE

```
%%Compressed Air Energy Storage-
%%Euler Numerical Integration
%%Author Mike Beeman
function h = CAES_Simulator_workingcopy(h)

%Determines whether to record the Turbine or Compressor Code
device = h.device;

%+++++++++++++++++++++++++++++++++++++++++++++++++++++++++++++++++++++++++++++++
%Default Variables
%+++++++++++++++++++++++++++++++++++++++++++++++++++++++++++++++++++++++++++++++

if h.Set_Variables.Default_Variables

C_Eff = .85;
T_Eff = .90;

%Experimental Limits In UoU Experiment
depth = 1100; % m
Win_LP = 100000; % kJ/s
Win_HP = 100000; % kJ/s
Wout_HP = 100000; % kJ/s
Wout_LP = 100000; % kJ/s
Miles = 13;
Volume = 100000; % m^2

%Ambient Conditions
Pamb = 70.55; %101; % kPa
Tamb =  20+273.15;
Absolute_Humidity_Amb = .02; %kg H2O vapor/kg dry air
row = 0;

%Conditions in tank at 0 psig
Ptank_low_lim = Pamb + 600*6.895; %600*6.895;
% Ptank_initial = Pamb;
Ttank = 44.5 + 273.15; %Kelvin
Ttank_in =  33.3+273.15;
%Conditions in tank at 200 psig
Ptank_high_lim = Pamb + 1100*6.895; %1100*6.895;
%T_T_in = 600 + 273.15; %Temperature Turbine Inlet

%Pressures Between HP and LP Turbine and Compressors
P_T_in_LP = Pamb + 100*6.895;
P_C_in_HP = Pamb + 200*6.895;

%Equipment Limits
T_C_in_HP = 200 + 273.15;
T_T_in_HP = 586 + 273.15;
T_T_in_LP = 586 + 273.15;

%Efficiencies
Np_T = .97;  %Turbine Polytropic
Np_C = .97;  %Compressor Polytropic

else
```

```
%++++++++++++++++++++++++++++++++++++++++++++++++++++++++++++++++++++++++++++++
%User Defined Variables
%++++++++++++++++++++++++++++++++++++++++++++++++++++++++++++++++++++++++++++++

%Experimental Limits
Volume = h.Set_Variables.Volume;
depth = h.Set_Variables.depth;
depth = depth*.3048; % m
Win_HP = h.Set_Variables.Win_HP; % kJ/s
Win_LP = h.Set_Variables.Win_LP; % kJ/s
Wout_HP = h.Set_Variables.Wout_HP; % kJ/s
Wout_LP = h.Set_Variables.Wout_LP;
% del_time = get(h.Set_Variables.,'Value');

%Ambient Conditions
Pamb = h.Set_Variables.Pamb; % kPa
Tamb = h.Set_Variables.Tamb;
Absolute_Humidity_Amb = h.Set_Variables.Absolute_Humidity; %kg H2O vapor/kg dry air

%Conditions in tank at 600 psi
Ptank_low_lim = h.Set_Variables.Ptank_low_lim;
Ttank = h.Set_Variables.Ttank; %Kelvin

%Conditions in tank at 1100 psi
Ptank_high_lim = h.Set_Variables.Ptank_high_lim;
T_T_in = h.Set_Variables.T_T_in; %Temperature Turbine Inlet

%Equipment Limits
T_C_in_HP = h.Set_Variables.T_C_in_HP;%Kelvin
T_T_in_HP = h.Set_Variables.T_T_in_HP;%Kelvin
T_T_in_LP = h.Set_Variables.T_T_in_LP;%Kelvin

%Pressures Between HP and LP Turbine and Compressors
P_T_in_LP = h.Set_Variables.P_T_in_LP;%kPa
P_C_in_HP = h.Set_Variables.P_C_in_HP;%kPa

%Efficiencies
Np_T = h.Set_Variables.Np_T;  %Turbine Polytropic
Np_C = h.Set_Variables.Np_C;  %Compressor Polytropic

end

%Ideal Gas Constants
cp_air = 1.005; %kJ/kg K
cv_air = 0.718; %kJ/kg K
cp_h2o_vapor = 4.18; %kJ/kg K
cv_h2o_vapor = 1.8723; %kJ/kg K

%Determines Time Units
del_time = 60;
if del_time == 60
   time_units = '(min)';
elseif del_time == 1
   time_units = '(sec)';
elseif del_time == 3600
   time_units = '(hrs)';
```

```
end

%++++++++++++++++++++++++++++++++++++++++++++++++++++++++++++++++++++++++++++++
%Compression Cycle
%++++++++++++++++++++++++++++++++++++++++++++++++++++++++++++++++++++++++++++++
% Note: Mass flowrates are determined by the HP Compressor and must be
% determined before LP Compression values can be found. Must also perform a
% saturation test to determine intensive properties of the air entering HP
% compressor after it has been cooled in Heat Exchanger

%First Stage Heat Exchanger Saturation Test
%========================================
[Pg Latent_Heat_Vaporization] = Saturation_Data_P(T_C_in_HP);
Relative_Humidity = Absolute_Humidity_Amb*P_C_in_HP/((.622 + Absolute_Humidity_Amb)*Pg);
if  Relative_Humidity > 1
   Absolute_Humidity = .622*Pg*Relative_Humidity/(P_C_in_HP-Relative_Humidity*Pg);
   'Cooling during compression cycle 1st stage Xchanger creates condensation.'
else
    Absolute_Humidity = Absolute_Humidity_Amb;
   'Cooling during compression cycle 1st stage Xchanger does not create condensation.'
end
Absolute_Humidity_HP_C = Absolute_Humidity;
Absolute_Humidity_LP_C = Absolute_Humidity_Amb;

%=============================================================================
%HP Compressor
%=============================================================================

%Ideal Gas Constants
%======================
cp = 1/(1+Absolute_Humidity)*cp_air + Absolute_Humidity/(1+Absolute_Humidity)*cp_h2o_vapor;
%cp humid air
cv = 1/(1+Absolute_Humidity)*cv_air + Absolute_Humidity/(1+Absolute_Humidity)*cv_h2o_vapor;
%cv humid air
R = cp - cv;
R_2 = R;
k = cp/cv;
k_coef = (k-1)/k;

%HP Compressor Initializations
%======================
Pexit(1) = Ptank_low_lim;
r(1) = Pexit(1)/P_C_in_HP;
r_2 = r(1);
P(1) = Ptank_low_lim;
Np_c = fzero(@(x)Np_C-(x)*(r(1)^k_coef-1)/(r(1)^(k_coef*x)-1),1);
y_coef_C_2 = k_coef*Np_c;
mass_flowrate(1) = Win_HP*C_Eff/(R*T_C_in_HP/(y_coef_C_2)*(r(1)^y_coef_C_2-1));
m(1) = P(1)*Volume/(R*Ttank);
T(1) = Ttank;
Texit(1) = T_C_in_HP*r(1)^(y_coef_C_2);
Q_C_out_HP(1) = mass_flowrate(1)*cp_air*(Texit(1)-Ttank_in);
n = 1;

%HP Compressor
%======================
```

```
while P(n) < Ptank_high_lim %m(n) < m_tank_final
   m(n+1) = m(n) + del_time*mass_flowrate(n);
   T(n+1) = (Ttank_in*mass_flowrate(n)*del_time*k +
T(n)*m(n))/(m(n)+mass_flowrate(n)*del_time);
   P(n+1) = m(n+1)*R*T(n+1)/(Volume);
   r(n+1) = P(n+1)/P_C_in_HP;
   mass_flowrate(n+1) = Win_HP*C_Eff/(R*T_C_in_HP/(y_coef_C_2)*(r(n+1)^y_coef_C_2-1));
   Texit(n+1) = T_C_in_HP*r(n+1)^(y_coef_C_2);
   n = n+1;
end

%Final Tank Temp
%===============
Ttankfinal = T(end)

%=========================================================================

%Listed Variables
%======================
t = 1:n;
run_time_Compressor = n*del_time;

%=========================================================================
% First Stage Heat Exchanger
%=========================================================================

%Mass flowrates of the Vapor, Condensation and Dry air
%=====================================================
mass_flowrate_Vapor_C_Hot = mass_flowrate*Absolute_Humidity_Amb/(…
Absolute_Humidity_Amb + 1); %Mass of H2O vapor before cooling.
mass_flowrate_Vapor_C_Cool = mass_flowrate*Absolute_Humidity/(Absolute_Humidity + 1);
%Mass of H2O vapor after cooling.
mass_flowrate_Air_C_Hot = mass_flowrate/(Absolute_Humidity_Amb + 1);
%Mass of dry air before cooling.
mass_flowrate_Air_C_Cool = mass_flowrate/(Absolute_Humidity + 1);
%Mass of dry air after cooling.
mass_flowrate_condensation = mass_flowrate_Vapor_C_Hot - mass_flowrate_Vapor_C_Cool;
%Mass condensed during cooling.

%Latent Heat If Condensation Occurs
%==================================
if  Relative_Humidity > 1
Psat_stage1_C = Absolute_Humidity_Amb*P_C_in_HP/((Absolute_Humidity_Amb + …
0.622)*Relative_Humidity);
[Tsat Latent_Heat_Vaporization] = Saturation_Data_T(Psat_stage1_C);
Q_Latent_Heat = mass_flowrate_condensation*Latent_Heat_Vaporization;
else
  Q_Latent_Heat = 0;
end
%=========================================================================


%=========================================================================
%LP Compressor
%=========================================================================
```

```
%LP Compressor Ideal Gas Constants
%======================
cp = 1/(1+Absolute_Humidity_Amb)*cp_air + …
Absolute_Humidity_Amb/(1+Absolute_Humidity_Amb)*cp_h2o_vapor %cp humid air
cv = 1/(1+Absolute_Humidity_Amb)*cv_air + …
Absolute_Humidity_Amb/(1+Absolute_Humidity_Amb)*cv_h2o_vapor %cv humid air
R = cp - cv;
R_1 = R;
Ramb_air = R;
k = cp/cv
k_coef = (k-1)/k;          %{Polytropic
Np_c = fzero(@(x)Np_C-(x)*(r(1)^k_coef-1)/(r(1)^(k_coef*x)-1),1);
y = 1/(1-k_coef*Np_c)
y_coef_C_1 = (y-1)/y;

%LP Compressor
%======================
Texit_C_LP = Tamb*(P_C_in_HP/Pamb)^(y_coef_C_1);
Win_LP = mass_flowrate/(C_Eff)*(R*Tamb/(y_coef_C_1)*((P_C_in_HP/Pamb)^y_coef_C_1-1));
del_T = Texit_C_LP-T_C_in_HP;
Q_C_out_LP = mass_flowrate.*del_T*cp + Q_Latent_Heat;

%Efficiency Parameters
%======================
W_Compressor = ((Win_HP)*run_time_Compressor+sum(Win_LP)*del_time);
W_Compressor_Watts = Win_HP + sum(Win_LP)/run_time_Compressor;
%=========================================================================

%=========================================================================
% Second Stage Heat Exchanger
%=========================================================================

%Obtains Tsat at the exit pressure of the HP Compressor
%=======================================================
Pv = P.*Absolute_Humidity/(.622+Absolute_Humidity);
[Tsat Latent_Heat_Vaporization] = Saturation_Data_T(Pv);

%Determines Latent Heat If Condensation Occurs
%==================================
for i = 1:n
   Q_Xchanger_2nd_St(i) = cp*mass_flowrate(i)*(Texit(i)-Ttank_in);
if Texit(i) < Tsat(i)
   [Pg Latent_Heat_Vaporization] = Saturation_Data_P(Texit(i));
   Absolute_Humidity_Tank(i) = .622*Pg/(P(i)-Pg);
   mass_flowrate_Vapor_C_Hot = mass_flowrate(i)*Absolute_Humidity/(Absolute_Humidity + 1);
%Mass of H2O vapor before cooling.
   mass_flowrate_Vapor_C_Cool =
mass_flowrate(i)*Absolute_Humidity_Tank/(Absolute_Humidity_Tank + 1); %Mass of H2O vapor
before cooling.
   mass_flowrate_condensation(i) = mass_flowrate_Vapor_C_Hot - mass_flowrate_Vapor_C_Cool;
%Mass condensed during cooling.
   Q_Latent_Heat_2nd_St(i) = mass_flowrate_condensation(i)*Latent_Heat_Vaporization;
   Q_Xchanger_2nd_St(i) = cp*mass_flowrate(i)*(Texit(i)-Ttank);
   Condesation_Test_2nd_St = 1;
else
   Q_Latent_Heat_2nd_St(i) = 0;
```

```
   Absolute_Humidity_Tank(i) = Absolute_Humidity;
   Condesation_Test_2nd_St = 0;
end
end

%Absolute Humidity in Tank
%========================
mass_flowrate_Vapor_In_Tank =
mass_flowrate.*Absolute_Humidity_Tank./(Absolute_Humidity_Tank + 1);
%Mass of H2O vapor before cooling.
mass_Vapor_In_Tank = sum(mass_flowrate_Vapor_In_Tank)*del_time;
Absolute_Humidity_Tank = mass_Vapor_In_Tank/(sum(mass_flowrate_Air_C_Hot)*del_time);
Absolute_Humidity = Absolute_Humidity_Tank;

%Ideal Gas Constants
%======================
cp = 1/(1+Absolute_Humidity)*cp_air + Absolute_Humidity/(1+Absolute_Humidity)*cp_h2o_vapor;
%cp humid air
cv = 1/(1+Absolute_Humidity)*cv_air + Absolute_Humidity/(1+Absolute_Humidity)*cv_h2o_vapor;
%cv humid air
R = cp - cv;

%Displays if Condensation Occurs
%================================
if Condesation_Test_2nd_St
   'Cooling during compression cycle 2nd stage Xchanger creates condensation.'
else
   'Cooling during compression cycle 2nd stage Xchanger does not create condensation.'
end

%=============================================================================
% CAES Viewer Variables
%=============================================================================

%Thermal Loads on HeatXchanger
%======================
Q_Xchanger_2nd_St = Q_Xchanger_2nd_St + Q_Latent_Heat_2nd_St;

Q_Energy_In = (sum(Q_C_out_LP)+sum(Q_Xchanger_2nd_St))*del_time*1e-6;

%Sets Plot Variables to Compressor
%================================
if device == 2
h.Plot_Variables = [t' T' P' mass_flowrate' m' Win_LP' Texit' Q_Xchanger_2nd_St' Q_C_out_LP'];
h.Variable_Label = {['time ' time_units], 'T(K)', 'P(kPa)', 'm/s (kg/s)',...
   'm (kg)', 'W(kW)', 'T(K)', 'Q(kW)', 'Q(kW)'};
h.title = {'Tank Temp (K)', 'Tank Pressure (kPa)', 'Mass Flow Rate (kg/s)',...
   'Mass in Tank (kg)', '      LP Compressor Work (kW) ', 'Exit Temp (K)', '          Q from HP…
Compressor (kW)', '          Q from LP Compressor (kW)'};
end

%Sets Plot Variables to HeatXchanger
%================================
if device == 3
h.Plot_Variables = [t' T' P' mass_flowrate' m' r' Texit' Q_C_out_HP' Q_C_out_LP'];
h.Variable_Label = {['time ' time_units], 'T(K)', 'P(kPa)', 'm/s (kg/s)',...
```

```
   'm (kg)', 'r', 'T(K)', 'Q(kW)', 'Q(kW)'};
h.title = {'Tank Temp (K)', 'Tank Pressure (kPa)', 'Mass Flow Rate (kg/s)',...
   'Mass in Tank (kg)', 'Pressure Ratio', 'Exit Temp (K)', '         Q from HP Compressor (kW)', '…
Q from LP Compressor (kW)'};
end

%=========================================================================

clear P Texit T r mass_flowrate time m n t
%+++++++++++++++++++++++++++++++++++++++++++++++++++++++++++++++++++++++++

%+++++++++++++++++++++++++++++++++++++++++++++++++++++++++++++++++++++++++
%Expansion Cycle
%+++++++++++++++++++++++++++++++++++++++++++++++++++++++++++++++++++++++++

%=========================================================================
%HP Turbine
%=========================================================================

%Ideal Gas Constants
%======================
cp = 1/(1+Absolute_Humidity)*cp_air + Absolute_Humidity/(1+Absolute_Humidity)*cp_h2o_vapor;
%cp humid air
cv = 1/(1+Absolute_Humidity)*cv_air + Absolute_Humidity/(1+Absolute_Humidity)*cv_h2o_vapor;
%cv humid air
R = cp - cv;
k = cp/cv;
k_coef = (k-1)/k;

%HP Turbine Initializations
%==========================
%Pin(1) = Ptank_high_lim*(T_T_in_HP/Ttankfinal)^(1/k_coef)
%r(1) = P_T_in_LP/Pin(1);
r(1) = P_T_in_LP/Ptank_high_lim;
Np_t = fzero(@(x)Np_T-(1/x)*(1-r(1)^(k_coef*x))/(1-r(1)^k_coef),.5);
 %Turbine Polytropic Coefficient
y_coef_T = k_coef*Np_t;
mass_flowrate(1) = Wout_HP/((T_Eff*R*T_T_in_HP/y_coef_T)*(1-r(1)^y_coef_T));
T(1) = Ttankfinal;
m(1) = Ptank_high_lim*Volume/(R*T(1));
P(1) = Ptank_high_lim;
Texit(1) = T_T_in_HP*r(1)^(y_coef_T);
Q_T_in_HP(1) = mass_flowrate(1)*cp*(T_T_in_HP-T(1));
clear n
n = 1;
Q_Expansion = Q_T_in_HP(1);

%HP Turbine
%======================
while P > Ptank_low_lim
   m(n+1) = m(n) - del_time*mass_flowrate(n);
   T(n+1) = (-T(n)*mass_flowrate(n)*del_time*k + T(n)*m(n))/m(n+1);
   P(n+1) = m(n+1)*R*T(n+1)/(Volume);
   r(n+1) = P_T_in_LP/P(n+1);
   mass_flowrate(n+1) = Wout_HP/(T_Eff*R*T_T_in_HP/y_coef_T*(1-r(n+1)^y_coef_T));
   Texit(n+1) = T_T_in_HP*r(n+1)^(y_coef_T);
```

```
   Q_T_in_HP(n+1) = mass_flowrate(n+1)*cp*(T_T_in_HP-T(n+1));
   Q_Expansion = Q_T_in_HP(n+1) + Q_Expansion;
   n = n+1;

   %This IF statement checks to ensure the Heat Energy Added during
   %expansion does not exceed that extracted during compression
   if Q_Expansion > Q_Energy_In*1E6
      %error('The HP Turbine Heat exchanger has exceeded the maximum heating capacity.  For…
adiabatic conditions reconfigure the boundary conditions used and run the simulation again.')
   end


end
%=========================================================================

%HP Turbine Saturation Test
%======================
clear Pv
Pv = Absolute_Humidity*P_T_in_LP/(Absolute_Humidity+.622);
[Tsat Latent_Heat_Vaporization] = Saturation_Data_T(Pv); %Test lowest Texit value for…
condensation.
clear j
j = 1;
while Texit(j) >= Tsat
   j = j+1;
   if j == length(Texit)
      break
   end
end
if Texit(j) < Tsat
   Absolute_Humidity = .622*Pv/(P_T_in_LP-Pv);
   'Cooling during HP expansion creates condensation.'
end
if j >= length(Texit)
   'Cooling during HP expansion does not create condensation.'
end
Absolute_Humidity_HP_T = Absolute_Humidity;

%LP Turbine
%==========================
del_T_T = T_T_in_LP-Texit;
Q_T_in_LP = mass_flowrate.*del_T_T*cp;
Texit_T_LP = T_T_in_LP*(Pamb/P_T_in_LP)^(y_coef_T);
Wout_LP = mass_flowrate.*T_Eff*(R*T_T_in_LP/y_coef_T*(1-(Pamb/P_T_in_LP)^y_coef_T));

%Saturation Test
%======================
[Pg Latent_Heat_Vaporization] = Saturation_Data_P(min(Texit_T_LP)); %Test lowest Texit…
value for condensation.
Relative_Humidity = Absolute_Humidity*Pamb/((.622 + Absolute_Humidity)*Pg);
if  Relative_Humidity > 1
   Absolute_Humidity = .622*Pg/(Pamb-Pg);
   'Cooling during LP expansion creates condensation.'
else
    Absolute_Humidity = Absolute_Humidity_Amb;
   'Cooling during LP expansion does not create condensation.'
```

```
end
Absolute_Humidity_LP_T = Absolute_Humidity;

%Listed Variables
%======================
t = 1:n;
run_time_Turbine = n*del_time;
W_Turbine = (Wout_HP*run_time_Turbine+sum(Wout_LP)*del_time);
W_Turbine_Watts = (Wout_HP+sum(Wout_LP)/run_time_Turbine);
Energy_per_Volume = W_Turbine/Volume;
Q_Energy_Out = (sum(Q_T_in_LP)+sum(Q_T_in_HP))*del_time*1e-6;
CAES_Efficiency = W_Turbine/W_Compressor*100


%Sets Plot Variables to Turbine Values
%================================
if device == 1
h.Plot_Variables = [t' T' P' mass_flowrate' m' Wout_LP' Texit' Q_T_in_HP' Q_T_in_LP'];
h.Variable_Label = {['time ' time_units], 'T(K)', 'P(kPa)', 'm/s (kg/s)',...
   'm (kg)', 'W(kW)', 'T(K)', 'Q(kW)', 'Q(kW)'};
h.title = {'Tank Temp (K)', 'Tank Pressure (kPa)', 'Mass Flow Rate (kg/s)',...
   'Mass in Tank (kg)', 'LP Turbine Work (kW)', 'Exit Temp (K)', '          Q into HP Turbine (kW)'…
,       Q into LP Turbine (kW)'};
end

%++++++++++++++++++++++++++++++++++++++++++++++++++++++++++++++++++++++++++++++
%Data Preperation for CAES_Viewer
%++++++++++++++++++++++++++++++++++++++++++++++++++++++++++++++++++++++++++++++

%Passes Listbox Variables
%=========================
h.List_Variables = strvcat(['Compressor Run Time (sec) = ' num2str(run_time_Compressor)],...
   ['Turbine Run Time (sec) = ' num2str(run_time_Turbine)],...
   ['Work in Compressor (GJ)= ' num2str(W_Compressor*1E-6)], ...
   ['Work out Turbine (GJ)= ' num2str(W_Turbine*1E-6)], ...
   ['CAES Plant Efficiency = ' num2str(CAES_Efficiency)],...
   ['Energy/Volume (kJ/m^3) = ' num2str(Energy_per_Volume)],...
   ['Heat Exchanger Energy Input (GJ) = ' num2str(Q_Energy_In)],...
   ['Heat Exchanger Energy Output (GJ) = ' num2str(Q_Energy_Out)]) ;

%Passes Plot Variables
%=======================
h.Schematic_Variables.one = strvcat([num2str(Pamb) ' kPa'], [num2str(Tamb) ' K']);
h.Schematic_Variables.two = strvcat([num2str(sum(Win_LP)/1000) ' MW LP Compressor'],..
[num2str(Win_HP*run_time_Compressor/1000) ' MW HP Compressor']);
h.Schematic_Variables.three = strvcat([num2str(sum(Wout_LP)/1000) ' MW LP Expander'],…
[num2str(run_time_Turbine*Wout_HP/1000) ' MW HP Expander']);
h.Schematic_Variables.four = strvcat([num2str(Ptank_high_lim) ' kPa']); %, [num2str(Ttank 'K']);
h.Schematic_Variables.five = strvcat([num2str(P_C_in_HP) ' kPa'], [num2str(Texit_C_LP) ' K']);
h.Schematic_Variables.six = strvcat([num2str(T_C_in_HP) ' K']);
h.Schematic_Variables.seven = strvcat([num2str(T_T_in_HP) ' K']); %[num2str(Pamb) ' kPa'],
h.Schematic_Variables.eight = strvcat([num2str(P_T_in_LP) ' kPa'], [num2str(T_T_in_LP) ' K']);
h.Schematic_Variables.nine = strvcat([num2str(Texit_T_LP) ' K']);
h.Schematic_Variables.ten = strvcat([num2str(CAES_Efficiency) ' %']);
```

```
%=========================================================================
% Saturation_Data_P
% Recieves a temperature and passes a saturation pressure
% and latent heat at that temperature.
function [P,Latent_Heat] = Saturation_Data_P(T)
[Temp_sat Psat hfg] = textread('Saturated Water Temperature Table.txt',...
   '%f %f %*f %*f %*f %*f %*f %*f %*f %f','headerlines',1);
% Opens Saturated Water Tables

Temp_sat = Temp_sat + 273.15;

% Scan table for interpolation data
%==================================
n = 1;
while T > Temp_sat(n) && T > Temp_sat(n+1)
   n = n+1;
end
Latent_Heat = hfg(n);

%Interpolate to find Pv
%=======================
P = (T-Temp_sat(n))/(Temp_sat(n+1)-Temp_sat(n))*(Psat(n+1)-Psat(n))+Psat(n);
h = (T-Temp_sat(n))/(Temp_sat(n+1)-Temp_sat(n))*(hfg(n+1)-hfg(n))+hfg(n);

%=========================================================================

%=========================================================================
% Saturation_Data_T
% Recieves a vapor pressure and passes a saturation
% temperature at that vapor pressure.
function [T,hfg] = Saturation_Data_T(Pv)
[Temp_sat Psat hf hg] = textread('Saturated Water Temperature Table.txt',...
   '%f %f %*f %*f %*f %*f %*f %f %f %*f %*f','headerlines',1);
% Opens Saturated Water Tables


Temp_sat = Temp_sat + 273.15;

for i = 1:length(Pv)
% Scan table for interpolation data
%==================================
n = 1;
while Pv(i) > Psat(n) && Pv(i) > Psat(n+1)
  n = n+1;
end

%Interpolate to find Pv
%=======================
T(i) = (Pv(i)-Psat(n))/(Psat(n+1)-Psat(n))*(Temp_sat(n+1)-Temp_sat(n))+Temp_sat(n);
hff = (T(i)-Temp_sat(n))/(Temp_sat(n+1)-Temp_sat(n))*(hf(n+1)-hf(n))+hf(n);
hgg = (T(i)-Temp_sat(n))/(Temp_sat(n+1)-Temp_sat(n))*(hg(n+1)-hf(n))+hg(n);
hfg = hgg-hff;
end
%=========================================================================

%=========================================================================
```

```
% Saturation_Data_S
% Recieves a temperature and passes an entropy at that temperature.
function [T,h] = Saturation_Data_S(T)
[Temp_sat Psat hf hg] = textread('Saturated Water Temperature Table.txt',...
    '%f %f %*f %*f %*f %*f %f %f %*f %*f','headerlines',1);
% Opens Saturated Water Tables

Temp_sat = Temp_sat + 273.15;
hfg = hg-hf;

% Scan table for interpolation data
%==================================
n = 1;
while Pv > Psat(n) && Pv > Psat(n+1)
  n = n+1;
end
%=========================================================================
```

APPENDIX B

EXPERIMENTAL EQUIPMENT

SPECIFICATIONS

Ashcroft® Pressure Transducer Connection Instructions

for use with HOBO® H22 and U30 Series Data Loggers

Applies to these Ashcroft Pressure Transducers:

Onset Part No.	Rating	Output	Ashcroft Part No.
T-ASH-G2-100	100 PSIG	0-5V representing 0 to 100 PSIG	G27M0205F2100#G-#4177
T-ASH-G2-200	200 PSIG	0-5V representing 0 to 200 PSIG	G27M0205F2200#G-#4177
T-ASH-G2-500	500 PSIG	0-5V representing 0 to 500 PSIG	G27M0205F2500#G-#4177

This document provides instructions on connecting the Ashcroft Pressure Transducers listed above to either the FlexSmart™ Analog Module used with HOBO H22 series data loggers or to the Analog Sensor Port option used with HOBO U30 series loggers. It also lists configuration values used by HOBOware® Pro software to configure the logger for each transducer. **Note:** For information on connecting the pressure transducer to the pressure source, and other transducer details, refer to the documentation provided by Ashcroft.

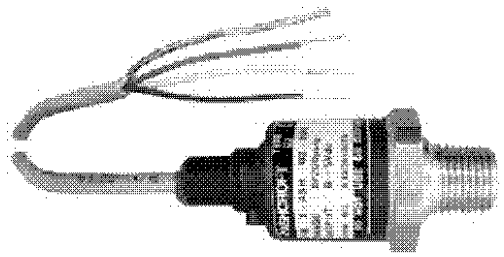

Ashcroft Pressure Transducer

Required:

- Selected Ashcroft Pressure Transducer
- HOBO H22 or U30 Series Data Logger
- FlexSmart Analog Module, Onset Part No: S-FS-CVIA (for H22 series) or Analog Sensor Port option (for U30 series)
- HOBOware Pro Software, version 2.2.1 or higher (2.4.0 or higher for U30 series)

Pressure Sensing Equipment Specifications

Operating range: -20° to 50°C (-4° to 122°F) with alkaline batteries
-40° to 60°C (-40° to 140°F) with lithium batteries

Sensor inputs: Three FlexSmart multi-channel modules and up to 6 Smart Sensors (which may have multiple parameters/channels)

Sensor connectors: Six RJ-12 Smart Sensor jacks plus 3 FlexSmart module slots

Communication: RS-232 via 3.5 mm serial port or/and 9-pin D-Sub connector

Dimensions: 15.6 cm x 8.4 cm x 4.6 cm (6.13" x 3.31" x 1.81")

Weight: 435 g (15.23 oz) with batteries 238 g (8.33 oz) without batteries

Memory: 512K nonvolatile flash data storage

Memory modes: Stop when full; wrap when full

Operational indicators: Six indicators provide logging and sensor network status

Logging interval: One second to 18 hours, user-specified interval (2-second minimum for two-channel S-FS-TRMSA operation)

Sensor excitation: 12 V DC at 200 mA total, with user-programmable warmup time on a per-channel basis

Battery life: One year typical use (up to 75 mA excitation with 10-minute or longer logging Interval and 1-second warmup time)

Battery type: Eight standard AA alkaline batteries included (for operating conditions -20°C/-4°F to 50°C/122°F); optional AA lithium batteries available for operating conditions of -40° to 60°C (-40° to 140°F).

External power: Supports optional 13.6 V DC regulated AC Wall Adapter Connector. Internal batteries may remain installed. Alternatively, an automotive battery or 9-12 V DC regulated Wall Adapter may be used, but it is recommended to remove the internal batteries since they will discharge to the level of the external supply.

Time accuracy: 0 to 2 seconds for the first data point and ±5 seconds per week at 25°C (77°F)

Logging mode: Immediate, timed delay, or trigger (button-push) start options; supports sampling intervals for some sensors

Data communication: Current readings while logging; read out while logging; read out when stopped

This product meets CE specification EN61326 criterion C for ESD, criterion C for Radiated Immunity, criterion B for Fast Transient, criterion A for Conducted Immunity, and criterion A for Power Frequency Magnetic Fields. To minimize measurement errors due to ambient RF, use the shortest possible probe sensor cable length.

Temperature Sensing Equipment

Description: OM-3000 Series dataloggers make taking measurements and downloading them to your PC for further analysis or archiving extremely easy. These dataloggers have a large integral backlit LCD display with graphics capabilities that can be used for on-the-spot measurements for all channels. Input ranges, user-defined session names and sampling intervals are easily programmed via the built-in keypad. With 128K memory, approximately 100,000 individual samples with date/time stamp can be stored in the datalogger for downloading. These dataloggers are powered from a rechargeable NiCad battery pack with a 1500 mA hour rating at 7.2 Vdc. The datalogger will operate for up to 13 hours with backlight off and up to 7 hours with backlight on. The unit may operate continuously if left connected to AC power. Datalogger setup is completely menu driven and is performed from the front panel tactile keypad. Datalogger main menu setup selections include channel setup, measure without recording setup, new recording setup, review data set, download data set, memory management, date and time setup, and also battery capacity check.

This unit has the following features:
24 Bit A/D Converter
J, K, T, and E Thermocouple Types
Four Channels
oC and oF User Selectable

This unit has the following specifications:
Number of Channels: 4 Thermocouple Inputs
Data Storage: 128K (100,000 samples)
Minimum Sampling Interval: 0.6 seconds for 4 Channels
Input Type:
J type T/C: -346 to 2183 oF (-210 to 1195 oC)
K type T/C: -418 to 2498 oF (-250 to 1370 oC)
T type T/C: -418 to 743 oF (-250 to 395 oC)
E type T/C: -418 to 1823 oF (-250 to 995 oC)
Voltage: ± 5 Vdc and ± 30 Vdc (user selectable)
Operating Time: 13 hrs with backlight off, 7 hrs with backlight on
Data Storage Format: up to 50 named data sets, up to 50 recordings per data set, up to 9,999 samples per recording

Thermocouple Probes

Quick Disconnect Thermocouples
with Miniature Connectors
Standard Dimensions

- Glass Filled Nylon Connector Body Rated to 220°C (425°F)
- 304, 310, 316, 321 SS, Inconel, or Super OMEGACLAD® XL Sheath
- Standard 6 and 12" Lengths Available†
- Sheath Diameters from 0.010 to 0.125"
- Grounded, Ungrounded, or Exposed Junction
- Color-Coded SMP Miniature Connector Termination
- Mating Connector, Cable Clamp, and Locking Clip Included FREE!
- LCP and Ceramic Connectors Available
- Custom Lengths Available

Available as SUPER OMEGACLAD™XL THERMOCOUPLE PROBES

See page A-43 to A-48.

ANSI color code shown

To order IEC color code see page A-9

OMEGACAL Factory Cal AVAILABLE

See Section Z

MADE IN USA

Starts at $24

MEETS OR EXCEEDS SPECIAL LIMITS OF ERROR (SLE) AND EN 60584-2: Tolerance Class 1

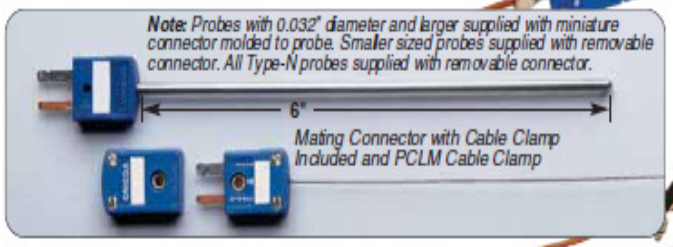

Note: Probes with 0.032" diameter and larger supplied with miniature connector molded to probe. Smaller sized probes supplied with removable connector. All Type-N probes supplied with removable connector.

Mating Connector with Cable Clamp Included and PCLM Cable Clamp

Shown smaller than actual size.

MOST POPULAR MODELS HIGHLIGHTED!

Standard Dimensions - Mini Quick Disconnect Probes

To Order *(Specify Model Number)*

Alloy/ANSI Color Code	Sheath Dia. inches	Model No. 6" Length	Price G*/E*	Price U*	Model No. 12" Length	Price G*/E*	Price U*	Price/Add'l 6"
Iron-Constantan 304 SS Sheath J	0.010	JMQSS-010(*)-6	$48.00	$68.00	JMQSS-010(*)-12	$49.25	$69.25	$1.25
	0.020	JMQSS-020(*)-6	28.00	30.00	JMQSS-020(*)-12	28.65	30.65	0.65
	0.032	JMQSS-032(*)-6	28.00	30.00	JMQSS-032(*)-12	28.65	30.65	0.65
	0.040	JMQSS-040(*)-6	28.00	30.00	JMQSS-040(*)-12	28.65	30.65	0.65
	0.062	JMQSS-062(*)-6	24.00	26.00	JMQSS-062(*)-12	24.80	26.80	0.80
	0.125	JMQSS-125(*)-6	24.00	26.00	JMQSS-125(*)-12	24.95	26.95	0.95

Electrical Power Sensing Equipment Equipment

FLUKE

Fluke 1735
Three-Phase Power Logger

Technical Data

Electrical load studies, energy consumption testing, and general power quality logging

The Fluke 1735 Three-Phase Power Logger is the ideal electrician or technician's tool for conducting energy studies and basic power quality logging. Set up the 1735 in seconds, with the included flexible current probes and color display. The 1735 logs most electrical power parameters, harmonics and captures voltage events.

- Record power and associated parameters for up to 45 days
- Monitor maximum power demand over user-defined averaging periods
- Prove the benefit of efficiency improvements with energy consumption tests
- Measure harmonic distortion caused by electronic loads
- Improve reliability by capturing voltage dips and swells from load switching
- Easily confirm instrument setup with color display of waveforms and trends
- Measure all three phases and neutral with included 4 flexible current probes
- View graphs and generate reports with included Power Log software
- Compact, rugged design with IP65 case, 600 V CAT III and two-year warranty

REFERENCES

[1] Crotogino, F., Mohmeyer, K.-U. and Scharf, R., *Huntorf CAES: More than 20 Years of Successful Operation, SMRI Spring Meeting 2001*, Orlando, 23.-24.04.2001, 2001, pp. 351-357.

[2] Gardner, John, Haynes, Todd, *Overview of Compressed Air Energy Storage*, Office of Energy Research, Policy and Campus Sustainability. ER-07-001. December 2007.

[3] Burroughs, Chris, *Solution to Some of Country's Energy woes Might be Little More than Hot Air*, Sandia Lab News (Online Publication), Vol. 53, No. 7, April 6, 2001.

[4] Bullough, Chris, *Advanced Adiabatic Compressed Air Energy Storage for the Integration of Wind*, European Wind Energy Conference, London UK, February 2004.

[5] Levine, Jonah, *Large Scale Electrical Energy Storage in Colorado,* CERI Research Group Report, June 30, 2007.

[6] Bullough, Chris, *Advanced Adiabatic Compressed Air Energy Storage for the Integration of Wind*, European Wind Energy Conference, London UK, February 2004.

[7] Burroughs, Chris, *Solution to Some of Country's Energy Woes Might be Little More than Hot Air*, Sandia National Laboratories: News Release, Vol. 53, No 7, April 6, 2001.

[8] Wark, Kenneth Jr., *Advanced Thermodynamics For Engineers*, McGraw-Hill, Inc, 1995, pp 21.

[9] Boyles, M., Cengel, Y., *Thermodynamics: An Engineering Approach 4^{rth} ed.*, Mc Graw Hill, 2004, pp 324-340, 406, 668-676.

[10] Ferzinger, J., Perić, *Computational Methods for Fluid Dynamics 3rd ed.*,Springer, 2002, pp 39-44.

[11] Lakshminarayana, B, *Fluid Dynamics and Heat Transfer of Turbomachinery*, John Wiley & Sons, 1996, pp 51-59.

[12] Cotton, William R.,Walko, Robert L., FLatau, Piotr J., *Polynomial Fits to Saturation Vapor Pressure*, Department of Atmospheric Science, Colorado State University, Fort Collins, Colorado, December 1992.

[13] *Measurement of Fluid Flow in Pipes Using Orifice, Nozzle, and Venturi*, American Society of Mechanical Engineers, ASME MFC-3M-1989, New York, January 31, 1980, pp 32-36.

[14] Incropera, Frank P., DeWitt, David P., *Fundamentals of Heat and Mass Transfer 5th Ed*, John Wiley and Sons, 2002, pp 241-246.

[15] Sara, Martin N., *Site Assessment and Remediation Handbook*, 2nd ed. Boca Ratone, FL: CRC Press LLC, 2003, pp 58.

[16] *Snowfall History*, Alta. 2009, Alta Ski Area, December 29, 2009, http://www.alta.com/pages/snowhistory.php.